

<https://helda.helsinki.fi>

---

## Epidermal mammalian target of rapamycin complex 2 controls lipid synthesis and filaggrin processing in epidermal barrier formation

Ding, Xiaolei

2020-01

---

Ding , X , Willenborg , S , Bloch , W , Wickström , S A , Wagle , P , Brodesser , S , Roers , A , Jais , A , Bruening , J C , Hall , M N , Rueegg , M A & Eming , S A 2020 , ' Epidermal mammalian target of rapamycin complex 2 controls lipid synthesis and filaggrin processing in epidermal barrier formation ' , Journal of Allergy and Clinical Immunology , vol. 145 , no. 1 , pp. 283-+ . <https://doi.org/10.1016/j.jaci.2019.07.033>

---

<http://hdl.handle.net/10138/323976>

<https://doi.org/10.1016/j.jaci.2019.07.033>

---

cc\_by\_nc\_nd

acceptedVersion

---

*Downloaded from Helda, University of Helsinki institutional repository.*

*This is an electronic reprint of the original article.*

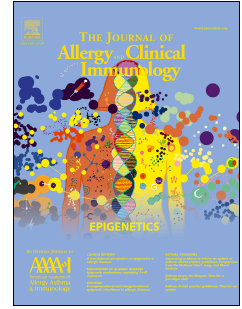
*This reprint may differ from the original in pagination and typographic detail.*

*Please cite the original version.*

# Journal Pre-proof

Epidermal mTORC2 controls lipid synthesis and filaggrin processing in epidermal barrier formation

Xiaolei Ding, PhD, Sebastian Willenborg, PhD, Wilhelm Bloch, PhD, Sara A. Wickström, MD, PhD, Prerana Wagle, MSc, Susanne Brodesser, PhD, Axel Roers, MD, Alexander Jais, PhD, Jens C. Brüning, MD, Michael N. Hall, PhD, Markus A. Rüegg, PhD, Sabine A. Eming, MD



PII: S0091-6749(19)31029-2

DOI: <https://doi.org/10.1016/j.jaci.2019.07.033>

Reference: YMAI 14119

To appear in: *Journal of Allergy and Clinical Immunology*

Received Date: 25 January 2019

Revised Date: 21 June 2019

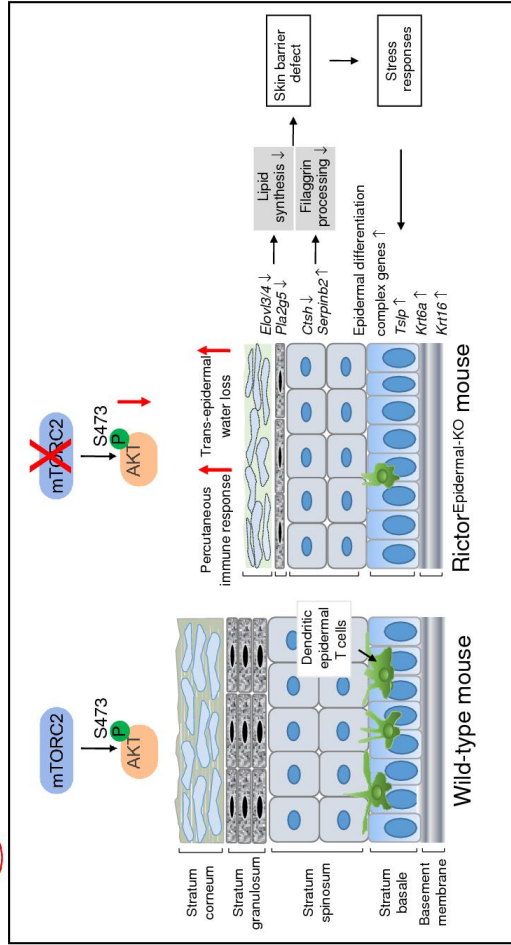
Accepted Date: 8 July 2019

Please cite this article as: Ding X, Willenborg S, Bloch W, Wickström SA, Wagle P, Brodesser S, Roers A, Jais A, Brüning JC, Hall MN, Rüegg MA, Eming SA, Epidermal mTORC2 controls lipid synthesis and filaggrin processing in epidermal barrier formation, *Journal of Allergy and Clinical Immunology* (2019), doi: <https://doi.org/10.1016/j.jaci.2019.07.033>.

This is a PDF file of an article that has undergone enhancements after acceptance, such as the addition of a cover page and metadata, and formatting for readability, but it is not yet the definitive version of record. This version will undergo additional copyediting, typesetting and review before it is published in its final form, but we are providing this version to give early visibility of the article. Please note that, during the production process, errors may be discovered which could affect the content, and all legal disclaimers that apply to the journal pertain.

© 2019 Published by Elsevier Inc. on behalf of the American Academy of Allergy, Asthma & Immunology.

 Epidermal mTORC2 Activity Controls Skin Barrier Function



bioRxiv

1 **Epidermal mTORC2 controls lipid synthesis and filaggrin processing in epidermal**  
2 **barrier formation**

3

4 Xiaolei Ding, PhD<sup>1,2</sup>, Sebastian Willenborg, PhD,<sup>1</sup> Wilhelm Bloch, PhD<sup>3</sup>, Sara A.  
5 Wickström, MD, PhD<sup>4,5,6,7</sup>, Prerana Wagle, MSc<sup>7</sup>, Susanne Brodesser, PhD<sup>7</sup>, Axel  
6 Roers, MD<sup>8</sup>, Alexander Jais, PhD<sup>9</sup>, Jens C. Brüning, MD<sup>2,7,9</sup>, Michael N. Hall, PhD<sup>10</sup>,  
7 Markus A. Rüegg, PhD<sup>10</sup>, Sabine A. Eming, MD<sup>1,2,7</sup>

8

9 <sup>1</sup>Department of Dermatology, University of Cologne, Kerpenerstr. 62, 50937 Cologne,  
10 Germany

11 <sup>2</sup>Center for Molecular Medicine Cologne (CMMC), University of Cologne, 50931  
12 Cologne, Germany

13 <sup>3</sup>Department of Molecular and Cellular Sport Medicine, German Sport University  
14 Cologne, 50933 Cologne, Germany

15 <sup>4</sup>Paul Gerson Unna Group 'Skin Homeostasis and Ageing', Max Planck Institute for  
16 Biology of Ageing, 50931 Cologne, Germany

17 <sup>5</sup>Helsinki Institute of Life Science, Biomedicum Helsinki, University of Helsinki, FI-  
18 00014 Helsinki, Finland

19 <sup>6</sup>Wihuri Research Institute, Biomedicum Helsinki, University of Helsinki, FI-00014  
20 Helsinki, Finland

21 <sup>7</sup>Cluster of Excellence Cellular Stress Responses in Aging-associated Diseases (CECAD),  
22 University of Cologne, 50931 Cologne, Germany

23 <sup>8</sup>Institute for Immunology, Medical Faculty Carl Gustav Carus, TU Dresden, 01307

24 Dresden, Germany

25 <sup>9</sup>Max Planck Institute for Metabolism Research, Gleueler Strasse 50, 50931 Cologne,

26 Germany

27 <sup>10</sup>Biozentrum, University of Basel, CH-4056 Basel, Switzerland

28

29 Corresponding author:

30 Sabine A. Eming, MD

31 Professor of Dermatology

32 Department of Dermatology

33 University of Cologne

34 Kerpenerstr. 62

35 50937 Cologne

36 Germany

37 Phone: ++49-221-4783196

38 Fax: ++49-221-4785949

39 E-mail: [sabine.eming@uni-koeln.de](mailto:sabine.eming@uni-koeln.de)

40 Conflict of interest statement:

41 The authors have declared that no conflict of interest exists.

42 **Abstract**

43 **Background:** Perturbation of epidermal barrier formation will profoundly compromise  
44 overall skin function, leading to a dry and scaly, ichthyosis-like skin phenotype, which is  
45 the hallmark of a broad range of skin diseases, including ichthyosis, atopic dermatitis,  
46 and a multitude of clinical eczema variants. An overarching molecular mechanism that  
47 orchestrates the multitude of factors controlling epidermal barrier formation and  
48 homeostasis remains to be elucidated.

49 **Objective:** Here we highlight a specific role of mammalian target of rapamycin complex  
50 2 (mTORC2) signaling in epidermal barrier formation.

51 **Methods:** Epidermal mTORC2 signaling was specifically disrupted by deleting *Rictor*,  
52 encoding an essential subunit of mTORC2 in mouse epidermis ( $Ric^{EKO}$ ). Epidermal  
53 structure and barrier function were investigated by a combination of gene expression,  
54 biochemical, morphological and functional analysis in  $Ric^{EKO}$  and control mice.

55 **Results:**  $Ric^{EKO}$  newborns displayed an ichthyosis-like phenotype characterized by  
56 dysregulated epidermal *de novo* lipid synthesis, altered lipid lamellae structure, and  
57 aberrant filaggrin processing. Despite a compensatory transcriptional epidermal repair  
58 response, the protective epidermal function was impaired in  $Ric^{EKO}$  mice as revealed by  
59 increased transepidermal water loss, enhanced corneocyte fragility, decreased dendritic  
60 epidermal T cells, and an exaggerated percutaneous immune response. Restoration of  
61 Akt-Ser473 phosphorylation in mTORC2-deficient keratinocytes by expression of  
62 constitutive Akt rescued filaggrin processing.

63 **Conclusion:** Our findings reveal a critical metabolic signaling relay of barrier formation  
64 where epidermal mTORC2 activity controls filaggrin processing and *de novo* epidermal

65 lipid synthesis during cornification. Our findings provide novel mechanistic insights into  
 66 epidermal barrier formation and could open up new therapeutic opportunities to restore  
 67 defective epidermal barrier conditions.

68

69 **Key words:** Epidermal barrier, mTORC2, rictor, ichthyosis, filaggrin, epidermal lipid

70 synthesis

***Abbreviations used***

ACD:	Allergic contact dermatitis
AD:	Atopic dermatitis
CTSH:	Cathepsin H
DETCs:	Dendritic epidermal T cells
EDC:	Epidermal differentiation complex
FLG:	Filaggrin gene
FFA:	Free fatty acids
$\gamma\delta$ -TCR:	$\gamma\delta$ -T cell receptor
GSEA:	Gene set enrichment analysis
HPTLC:	High performance thin layer chromatography
IV:	Ichthyosis vulgaris
ICD:	Irritant contact dermatitis
Krt:	Keratin
LB:	Lamellar body
Lor:	Loricrin
mTORC1/2:	Mammalian target of rapamycin complex 1/2
myr-AKT:	Myristoylated Akt1
Rictor:	Rapamycin-insensitive companion of TOR
Ric <sup>EKO</sup> :	Epidermis-specific homozygous Rictor deletion
RNA-seq:	RNA-Sequencing
SB:	Stratum basale
SC:	Stratum corneum
SG:	Stratum granulosum
SS:	Stratum spinosum
TEM:	Transmission electron microscopy
TSLP:	Thymic stromal lymphopoietin
TEWL:	Transepidermal water loss

71

72 **Capsule Summary (35 words)**

73 An overarching molecular mechanism that orchestrates the multitude of factors  
74 controlling epidermal barrier formation remains to be elucidated. Here, we highlight a  
75 specific role of mTORC2 signaling in epidermal barrier function.

76

77 **Key Messages**

- 78 • The Ric<sup>EKO</sup> mouse develops an ichthyosis-like phenotype and might serve as a  
79 new preclinical disease model for studying epidermal barrier defects at the  
80 molecular level.
- 81 • Altered mTORC2 activity may represent a predisposing factor for skin disorders  
82 associated with disrupted epidermal barrier function.

83

84



## 85 **Introduction**

86 The epidermis is a stratified squamous epithelium that provides a life-sustaining  
87 permeability barrier preventing water loss and protecting the body from a plethora of  
88 physical and chemical insults as well as pathogenic microorganisms <sup>1</sup>. Perturbation of  
89 epidermal barrier function will profoundly compromise overall skin barrier function,  
90 frequently leading to a dry and scaly, ichthyosis-like skin phenotype, which is the  
91 hallmark of a broad range of skin diseases, including ichthyosis, atopic dermatitis (AD),  
92 and a multitude of clinical eczema variants associated for example with diabetes mellitus  
93 or aging <sup>2-4</sup>. Quality of life is frequently negatively affected and patients are also at high  
94 risk for associated morbidity and mortality <sup>5</sup>. The molecular mechanisms regulating  
95 proper barrier function and maintenance are not yet understood, and were the aim of this  
96 study.

97 The epidermal barrier function is acquired and maintained by a tightly regulated  
98 keratinocyte differentiation process, known as cornification. The innermost mitotically  
99 active cell layer, the stratum basale (SB), undergoes continuous proliferation and  
100 differentiation, providing cells to the above stratum spinosum (SS), stratum granulosum  
101 (SG), and the stratum corneum (SC). The outermost SC makes up most of the  
102 permeability barrier. The SC consists of flattened, anuclear and keratin-filled corneocytes  
103 embedded in an intercellular lipid-rich matrix composed of ceramides, cholesterol, and  
104 free fatty acids (FFA) in an acidic environment <sup>2, 6</sup>. Perturbation of cornification will  
105 profoundly compromise skin barrier function <sup>2, 6</sup>.

106 Genetic analyses have established a strong link between genetic defects and skin  
107 barrier disorders in both humans and mice, providing the basis for the current

108 understanding of molecular networks orchestrating cornification <sup>7</sup>. Of particularly  
109 importance was the discovery of the loss-of-function mutations in the filaggrin (*FLG*)  
110 gene, the cause of the most common genodermatosis, namely ichthyosis vulgaris, which  
111 is characterized by dry, scaly skin <sup>8-9</sup>. Ichthyosis vulgaris has been identified as a  
112 predisposing factor for the development of AD, the most common chronic inflammatory  
113 skin disease, affecting up to 20% of children and 7-10% of adults <sup>10</sup>. However, a  
114 significant number of AD patients have no *FLG* mutations and recent human genetic  
115 studies suggest that also a reduction of profilaggrin at the protein level can lead to skin  
116 barrier defects suggesting that other mechanisms and candidate molecules may regulate  
117 profilaggrin expression and proteolytic processing <sup>9, 11</sup>. Further, the identification of  
118 mutations in diverse *Elovl* genes in mouse and pediatric AD patients, encoding very-long-  
119 chain fatty acid elongases revealed a central role for *de novo* ceramide synthesis in  
120 cornification and proper epidermal barrier function <sup>1,10, 12-14</sup>. In addition, *Pla2g5* activity  
121 catalyzes FFA synthesis, and has been shown to be critical in epidermal barrier formation  
122 <sup>15</sup>. However, the overarching molecular mechanisms that orchestrate the multitude of  
123 factors controlling keratinocyte fate and cornification are not known <sup>16-17</sup>.

124         Recently, we identified the serine/threonine protein kinase mammalian (also  
125 known as mechanistic) target of rapamycin (mTOR) as an essential regulator of  
126 epidermal differentiation and barrier formation in embryonic development <sup>18-19</sup>. Here we  
127 hypothesized that mTORC2 plays a critical role in postnatal epidermal barrier assembly  
128 and maintenance. mTOR is a central regulator of cell growth and metabolism, and is  
129 evolutionarily highly conserved <sup>20-21</sup>. mTOR assembles in two structurally and  
130 functionally distinct, multi-protein complexes, referred to as mTORC1 and mTORC2 <sup>20-21</sup>.

131 The Rictor (rapamycin-insensitive companion of TOR) protein is an essential and specific  
132 subunit of mTORC2. Growth factors are able to stimulate mTORC2 kinase activity, and  
133 activated mTORC2 phosphorylates several members of the AGC kinase family, including  
134 AKT, specifically at Ser473 (AKT-pSer473) to control cell metabolism and cytoskeleton  
135 organization<sup>22-23</sup>. In keratinocyte differentiation, AKT activity is induced, regulating  
136 filaggrin expression and processing<sup>24-25</sup>. Interestingly, a recent study showed that  
137 increased Raptor expression, the regulatory associated protein of mTORC1 correlates  
138 with reduced AKT activity and filaggrin expression in the skin of AD patients<sup>26</sup>. In this  
139 study we assessed the role of epidermal mTORC2 in postnatal skin barrier function by  
140 inactivating *Rictor* in the epidermis in mice. We show that mTORC2 promotes non-  
141 redundant functions for proper cornification via regulation of epidermal lipid metabolism  
142 and filaggrin processing. Our findings could suggest a new therapeutic strategy to  
143 regulate epidermal barrier function and to prevent complications in patients with dry skin  
144 diseases.

145

**146 Methods****147 Mice**

148 Epidermal-specific *Rictor* knockout mice (C57BL/6) were generated by crossing mice  
149 carrying loxP-flanked *Rictor* alleles with a Cre-transgenic strain expressing Cre  
150 recombinase under control of the human K14 promoter (Supplemental Figure 1A)<sup>18</sup>.  
151 Littermates that either lacked Cre or expressed Cre but carried a heterozygous loxP-  
152 flanked *Rictor* allele served as controls. Genotyping was performed as previously  
153 described<sup>18</sup>. Mice were maintained and bred under standard pathogen-free conditions.  
154 All procedures were approved by the North Rhine-Westphalian State Agency for Nature,  
155 Environment, and Consumer Protection and the University of Cologne.

156

**157 Histological analysis**

158 Skin tissues were fixed in 4% PFA, embedded in paraffin, and sectioned (10  $\mu$ m).  
159 Hematoxylin and eosin staining was performed following a standard procedure<sup>27</sup>. Images  
160 were analyzed using a light microscope (Leica DM4000B, Leica Microsystems, Wetzlar,  
161 Germany).

162

**163 Separation of epidermis from mouse back skin**

164 The subcutaneous fat tissue was mechanically dissected from excised back skin. The  
165 epidermis was separated from the dermis after floating skin biopsies in 0.5 M ammonium  
166 thiocyanate (NH<sub>4</sub>SCN) in phosphate buffer, pH 6.8 (0.1 M NH<sub>2</sub>HPO<sub>4</sub>, 0.1 M KH<sub>2</sub>PO<sub>4</sub>) for  
167 30 min on ice, epidermis side up. The epidermis was used for either RNA isolation,  
168 biochemical analysis, or immunostaining.

169

**170 Immunostaining**

171 For immunohistochemical and immunofluorescence staining, cryosections from Optimal  
172 Cutting Temperature compound (OCT, Tissue Tek) embedded tissues were fixed (4%  
173 PFA or in methanol), blocked (10% normal goat serum in PBS), and incubated with  
174 primary antibodies (diluted in blocking buffer) overnight at 4°C. Bound primary antibody  
175 was detected by incubation with peroxidase-conjugated (EnVision System, Dako)  
176 secondary antibody followed by incubation with peroxidase substrate (Sigma) or Alexa-  
177 Fluor 488- or Alexa Fluor 594-conjugated antibodies (Invitrogen). Nuclei were  
178 counterstained with hematoxylin or 4,6-diamidino-2-phenylindole (DAPI, Invitrogen).  
179 After washing, slides were mounted in mounting medium. For whole-mount staining,  
180 epidermis was separated from ears as described above. Epidermal sheets were fixed by  
181 acetone and stained with anti- $\gamma\delta$ -TCR antibody. Images were taken with a Zeiss Meta 710  
182 Confocal Microscope or KEYENCE Fluorescence Microscope (BZ-9000). Antibody  
183 information can be found in Supplemental Table 1. For quantification of pAkt-S473  
184 staining, three representative HPFs/section were quantified using ImageJ software  
185 (<https://imagej.nih.gov/ij/index.html>) as described previously<sup>27</sup>. Findings are expressed as  
186 the percentage of pAkt-S473 stained areas within the ear epidermis. Numbers of  
187 inflammatory cells were determined by counting positively stained cells in five  
188 representative HPFs (400x)/section. Analyses were performed in a blinded manner by  
189 two independent investigators.

190

**191 Transmission electron microscopy**

192 Skin tissues were isolated and fixed in buffer (2% paraformaldehyde, 2% glutaraldehyde,  
193 0.1M cacodylate buffer at pH 7.35) and postfixed with ruthenium tetroxide. Tissue  
194 embedding and ultrathin section preparation were done as previously described <sup>28</sup>.

195

### 196 **Flow cytometry and cell sorting**

197 For analysis of immune cells, single-cell suspensions of skin from control and Ric<sup>EKO</sup>  
198 were prepared by a combination of enzymatic digestion (Liberase Blendzyme, Roche  
199 Applied Science) and mechanical disruption (Medimachine System, BD Biosciences) as  
200 previously described <sup>28</sup>. For flow cytometry analysis, cells were stained as described  
201 previously <sup>28</sup>. Briefly, cells were passed through a 40 µm cell strainer, washed with PBS,  
202 and incubated with the following antibodies: eFluor® 450- or APC-eFluor® 780-  
203 conjugated anti-CD45 (clone 30-F11, eBiosciences), APC-Cy7-conjugated anti-CD4  
204 (clone GK1.5, BD Pharmingen™), PE- or PE-Cy7-conjugated anti-CD3e (clone 145-  
205 2C11, eBiosciences), PE-conjugated anti-Siglec-F (clone E50-2440, BD Pharmingen™),  
206 FITC- or BV421-conjugated anti-γδ T-Cell Receptor (clone GL3, BD Pharmingen™),  
207 FITC-conjugated anti-Vγ3 TCR (clone 536, BD Pharmingen™), FITC-conjugated anti-  
208 F4/80 (clone Cl:A3-1, Bio-Rad) or APC-Cy7-conjugated Ly-6G (clone E50-2440, BD  
209 Pharmingen™) in FACS buffer. Dead cells were excluded using 7-amino-actinomycin D  
210 (7-AAD) (BD Biosciences). Cells were analyzed on a FACSCanto II flow cytometer  
211 (BD), which was equipped with FACSDiva software (BD). For flow cytometry sorting,  
212 GFP<sup>+</sup> keratinocytes were sorted by FACS Aria cell sorting system (BD).

213

### 214 **RNA transcriptomics and GSEA**

215 Total RNA was extracted from separated epidermal tissue using RNeasy Minikit (Qiagen)  
216 and RNA quality was determined using an Agilent 2200 TapeStation. Preparation of  
217 amplification reactions of complementary DNA (cDNA) was performed at the Cologne  
218 Center for Genomics (CCG) using Ovation RNA-Seq System V2 (NuGen) and library  
219 was prepared using the Nextera XT library preparation kit (Illumina). RNA sequencing  
220 was carried out on Illumina HiSeq2000 machines using the 2\_100-bp protocol and V3  
221 chemistry. After quality control, adapter sequences were removed by flexbar63. Reads  
222 mapping to ribosomal RNA-related genes were filtered out using a custom ribosomal  
223 RNA-only reference. After pre-processing, reads were mapped to the *Mus musculus*  
224 reference genome (build GRCm38\_79), followed by differential gene expression analysis  
225 using the DESeq2 R library (version 1.6.3). Hierarchical clustering was performed in *R*.  
226 Transcripts regulated greater than 1.5 fold with a *p* value of  $< 0.05$  were used in GO term  
227 analysis (DAVID Bioinformatics Resources 6.8) to identify enriched functional  
228 annotations. Gene set enrichment analysis was performed on whole gene list and  
229 compared to the Broad Institute Molecular Signatures Database collection of chemical  
230 and genetic perturbations (C2) using the Web-based tool available from the Broad  
231 Institute<sup>29</sup>. Enrichments with an FDR value  $< 0.05$  were considered significant.

232

### 233 **CE isolation for microscopy**

234 A defined area of dorsal mouse skin (25 mm<sup>2</sup>) was boiled in isolation buffer (20 mM  
235 Tris-HCl, pH 7.5, 5 mM EDTA, 10 mM DTT, and 2% SDS) under vigorous shaking for  
236 40 min. After centrifugation, the CEs were washed twice with isolation buffer and were  
237 analyzed using a hemocytometer<sup>30</sup>.

238

**239 Lipid analysis**

240 For the analysis of SC lipids, the SC was separated from the back skin of newborn mice  
241 by floating the skin with the dermis side down on 0.5% trypsin in phosphate buffered  
242 saline (PBS) for 24 h at 37 °C<sup>31</sup>. The SC was washed in PBS, lyophilized and weighed.  
243 Lyophilized SC was homogenized in 0.5 ml of water using the Precellys 24  
244 Homogenisator (Peqlab, Erlangen, Germany) at 6,500 rpm for 30 sec. After the addition  
245 of 0.5 ml of water and 2 ml of chloroform/methanol 1:2 (v/v), freely extractable SC lipids  
246 were extracted for 24 h at 37 °C and purified using a modification of the Bligh-Dyer  
247 procedure as previously described<sup>32</sup>. For lipid quantification, the equivalent of 1.1 mg of  
248 lyophilized SC was loaded on 20 × 10 cm HPTLC plates which were developed twice in  
249 chloroform/methanol/glacial acetic acid 190:9:1 (v/v/v). Quantitative analytical TLC  
250 determination was performed as previously described<sup>33</sup>. Nile red staining was performed  
251 on cryo-sections for 2 min with 0.2 mg/ml Nile red in 75% glycerol; the fluorescence  
252 intensity of Nile red stained epidermis was determined by integrated density using  
253 ImageJ software.

254

**255 Trans-epidermal water loss (TEWL) measurements**

256 TEWL measurements were carried out as described previously<sup>18</sup> using a Tewameter  
257 (Courage and Khazaka Electronic GmbH, Cologne, Germany) and the measurements  
258 were performed according to the manufacturer's instructions.

259

**260 Irritant and allergic contact dermatitis**



261 To assess irritant contact dermatitis (ICD), the inner and outer surface of right ear was  
262 treated with 5  $\mu$ l 1% croton oil in acetone/olive oil (4:1). The left ear was treated with  
263 acetone/olive oil only and taken as a control. Ear thickness was measured 4, 8, and 24 h  
264 after the treatment using a digital caliper. Ear swelling was determined by calculating the  
265 changes of ear thickness between challenged ear (right) and control ear (left). To evaluate  
266 hapten-induced allergic contact dermatitis (ACD), mice were sensitized by painting 25  $\mu$ l  
267 of 1% 1-fluoro-2,4-dinitrobenzene (DNFB) (Sigma) in acetone/olive oil (4:1) onto the  
268 shaved abdominal skin at day 0. At day 6, mice were challenged by applying 5  $\mu$ l 0.4%  
269 DNFB in acetone/olive oil on the inner and outer surface of right ear, respectively. The  
270 left ear was treated with acetone/olive oil only and taken as a control. Ear thickness was  
271 measured 8, 24, and 48 h after the treatment using a digital caliper. Ear swelling was  
272 determined by calculating the changes of ear thickness between challenged ear (right) and  
273 control ear (left).

274

### 275 **Cell culture**

276 Keratinocytes were isolated from newborns and cultured in low  $\text{Ca}^{2+}$  medium as  
277 described previously <sup>27</sup>. Briefly, skin was floated, dermal side down, on 0.25% trypsin  
278 solution (Gibco) for 16 h at 4°C. Epidermis was separated from the dermis and minced  
279 with a scalpel. Cell and epidermal tissue were suspended, shaken for 30 min at 37°C, and  
280 seeded on collagen-coated 6-well plates with mitomycin C- (Sigma) treated 3T3  
281 fibroblast feeder layer cells. For the induction of keratinocyte differentiation, the medium  
282 was supplemented with 0.2 mM  $\text{CaCl}_2$  (high  $\text{Ca}^{2+}$  medium).

283

**284 Plasmids, virus preparation, and keratinocyte infection**

285 MSCV-IRES-green fluorescent protein (GFP) retrovirus vector with myr-AKT was used  
286 as described previously<sup>34</sup>. myr-AKT-IRES-GFP and IRES-GFP retroviral supernatants  
287 were produced in 293T cells as previously described<sup>35</sup>. Briefly, 293T cells were  
288 transfected with vector constructs and packaging plasmids (pVPack-GP and pVPack-Eco;  
289 Stratagene). Forty-eight hours after transfection, virus supernatant was harvested and  
290 concentrated by precipitation with chondroitin 6-sulfate (CSC) (Sigma) and polybrene  
291 (Sigma), and centrifuged. Keratinocytes (P2) were exposed to concentrated viruses for 24  
292 h and GFP<sup>+</sup> cells were sorted by flow cytometry.

293

**294 qRT-PCR analysis**

295 RNA from epidermis and skin was extracted using an RNA isolation kit (Qiagen)  
296 according to the manufacturer's instructions. Reverse transcription of isolated RNA was  
297 performed using the High Capacity cDNA RT Kit (Applied Biosystems). Amplification  
298 reactions were performed with PowerSYBR Green PCR Master Mix (Applied  
299 Biosystems) using a 7300 Real Time PCRsystem (Applied Biosystems). The comparative  
300 method of relative quantification ( $2^{-\Delta\Delta Ct}$ ) was used to calculate the expression level of  
301 the target gene normalized to GAPDH. Primer sequence information can be found in  
302 Supplemental Table 2.

303

**304 Western blot analysis**

305 Epidermis was separated from the dermis and dissociated with a MixerMill. For analysis  
306 of filaggrin, loricrin and keratin epidermis was lysed in a 4% SDS lysis buffer.

307 Alternatively, cells or tissues were lysed in radio immunoprecipitation assay (RIPA)  
308 buffer, containing protease inhibitor (Sigma-Aldrich) and phosphatase inhibitor (Roche).  
309 Protein concentration was determined by Micro BCA Protein Assay Kit (Thermo  
310 Scientific) and 20 mg protein per sample was subjected to SDS-PAGE (Invitrogen).  
311 Subsequently, protein was blotted to PVDF membranes. After blocking (5% non-fat milk  
312 in TBST buffer), membranes were incubated with primary antibodies. Antibody  
313 information can be found in Supplemental Table 1. For densitometry analysis, enhanced  
314 chemiluminescence exposed film was scanned and quantified with ImageJ software.  
315 Briefly, images were converted to grayscale and the background was removed. The  
316 densitometry was achieved by Gel Analysis method with ImageJ software. The ratio of  
317 filaggrin monomer and total filaggrin, pro-filaggrin and  $\beta$ -actin were determined with  
318 control set to 1 or the relative intensity was calculated after normalizing to a loading  
319 control ( $\beta$ -actin).

320

### 321 **Statistical analysis.**

322 Data are presented as mean  $\pm$  s.e.m. and statistics was performed using PRISM software  
323 (GraphPad, version 5.0a). Statistical significance of difference was determined using  
324 unpaired 2-tailed Student's *t*-test or ANOVA one-way test analysis with Bonferroni  
325 multiple comparison test. *P* value  $<0.05$  was considered to be statistically significant.

326

327 **Results**328 **Ric<sup>EKO</sup> mice display a transient ichthyosis-like phenotype**

329 To explore the role of epidermal mTORC2 signaling, we knocked out *Rictor* specifically  
330 in the epidermis as previously described<sup>18</sup>. Briefly, mice carrying a loxP-flanked *Rictor*  
331 allele were crossed with a transgenic mouse expressing Cre recombinase under the  
332 control of the human keratin 14 (K14) promoter<sup>36-37</sup>, leading to epidermis-specific  
333 deletion of *Rictor* (Ric<sup>EKO</sup>) in all basal cells and their progeny (Supplemental Figure 1A).  
334 Epidermis-specific Cre-mediated recombination of floxed *Rictor* alleles, verified by PCR  
335 analysis of genomic DNA extracted from different organs including the epidermis,  
336 resulted in effective epidermal loss of Rictor protein expression as confirmed by Western  
337 blot analysis and immunohistochemical staining (Figure 1A and Supplemental Figure 1B  
338 and C). Immediately after birth, Ric<sup>EKO</sup> mice were clearly distinguishable from their  
339 wildtype littermates, exhibiting shiny, translucent and fragile skin. Occasionally, Ric<sup>EKO</sup>  
340 newborns showed small erosions at the trunk, which might have occurred due to  
341 mechanical stress of the skin during birth. This skin fragility may have led to the  
342 observed death of approximately 20% of the mutant mice before or after weaning  
343 (Supplemental Figure 1D). By day 7 (P7), a prominent phenotype of dry and scaly,  
344 ichthyosis-like skin was apparent, often beginning with scaling of the ventral side already  
345 around P3 (Figure 1B). Histological analysis revealed a stratified epidermis but  
346 significantly reduced epidermal thickness in Ric<sup>EKO</sup> pups at P4 (Figure 1C). Epidermal  
347 atrophy was primarily due to reduced granular cell layers and thinner SC. In addition, the  
348 SC in Ric<sup>EKO</sup> mice displayed structural defects including poor organization of upper SC  
349 layers and densely packing of lower ones compared with the well-defined basket weave-

350 like structure in controls (Figure 1C). Although less pronounced, the epidermal atrophy  
351 remained detectable in adults (P70) (Supplemental Figure 1E). Morphological alterations  
352 in the epidermis of Ric<sup>EKO</sup> newborns were paralleled by a transient impairment of  
353 epidermal barrier function as revealed by a significant increase in trans-epidermal water  
354 loss (TEWL) in P4 mutants (Figure 1D, Supplemental Figure 1F). As assessed by  
355 immunofluorescent staining for multiple tight/adherent junction proteins and components  
356 of desmosomal plaques, intercellular junctions appeared to be similar in control and  
357 Ric<sup>EKO</sup> epidermis (Supplemental Figure 1G). Ric<sup>EKO</sup> mice were born at the expected  
358 Mendelian ratio and exhibited normal body weight at birth, yet their weight by P5  
359 decreased by 20% compared with littermate controls; the smaller body size persisted  
360 throughout adulthood (Figure 1E, Supplemental Figure 1H).

361

### 362 **Ric<sup>EKO</sup> mice display increased corneocyte fragility**

363 To test whether epidermal atrophy and mechanical fragility in young Ric<sup>EKO</sup> mice was  
364 associated with decreased physical resistance of the SC, cornified envelopes (CE) were  
365 prepared from the back skin of control and Ric<sup>EKO</sup> mice at P5. Notably, 80% of CE  
366 isolated from control mice remained in a uniformly rigid, large and intact, polygonal  
367 shape, whereas more than 60% of Ric<sup>EKO</sup> CE were ruptured, irregular, and fragmented,  
368 which is indicative of significant fragility and structural defects (Figure 1F).

369 Ultrastructural analysis of P5 epidermis by transmission electron microscopy (TEM)  
370 showed that the inner portion of Ric<sup>EKO</sup> epidermis, including basement membrane,  
371 stratum basale and stratum spinosum, as well as desmosomal plaques were not grossly  
372 affected (Supplemental Figure 1I). However, detailed inspection revealed that keratin

373 intermediate filaments in the mutant mice were not condensed and were more loosely  
374 packed compared to controls (Figure 1G), which may contribute to the reduced resistance  
375 to mechanical stress in Ric<sup>EKO</sup> CE. Together, our findings demonstrate major structural  
376 defects in the formation of the SG and SC in the absence of epidermal mTORC2 activity.

377

378 **Epidermal mTORC2 deficiency induces a compensatory transcriptional epidermal**  
379 **repair program in Ric<sup>EKO</sup> mice**

380 To identify specific genes and pathways mediating mTORC2 signaling and orchestrating  
381 the SG to SC transition, we performed a RNA-sequencing (RNA-seq) transcriptome  
382 analysis of epidermis from mutant and control embryos at E19.5, when epidermal  
383 maturation nears completion and epidermal gene expression is not influenced by  
384 exposure to environmental insults that could mask primary mechanistic effects.

385 A one-way analysis of variance was performed to calculate the most variable and  
386 differentially expressed genes between both sets of epidermal tissue (fold change >2 and  
387 with *P* value < 0.05). Analysis revealed 231 and 249 genes down- and up-regulated,  
388 respectively, in Ric<sup>EKO</sup> epidermis versus controls (Figure 2A). To identify biological  
389 processes underlying the observed gene expression alterations, we performed Gene  
390 Ontology Enrichment analysis (GO) and Pathway Enrichment analysis of the  
391 differentially expressed genes at the 1.5-fold cut-offs using DAVID 6.8. The upregulated  
392 gene set was particularly enriched in genes involved in peptide cross-linking (e.g.  
393 *Lce3a/b*, *Sprr1a*, and *Sprr2h*), keratinization (e.g. *Krt6a*, *Krt16*), keratinocyte  
394 differentiation (e.g. *Sfn*, *Sprr1a*, *Lce3a*), and wound repair (e.g. *Krt6a*, *Krt16*, *S100a8*)  
395 among others. The downregulated gene set was highly enriched for immune regulators

396 (e.g. *Oas1f*) and lipid metabolism (e.g. *Elovl3/4*, *Pnpla5*, *Pla2g5*) (FDR < 0.05) (Figure  
397 2A and B). One of the most striking features of the RNA-seq data was the upregulation of  
398 genes for late keratinocyte differentiation and SC components, including small proline-  
399 rich proteins (Sprr), late cornified envelope proteins (Lce), and S100 proteins (Figure 2A).  
400 Several of these gene families comprise the epidermal differentiation complex (EDC),  
401 encoding a dense cluster of genes whose protein products have been identified as major  
402 molecular markers and important functional regulators for terminal differentiation in the  
403 stratified epidermis (Figure 2C) <sup>38</sup>. A panel of differentially regulated genes was  
404 confirmed by qRT-PCR-analysis, validating the RNA-seq data (Figure 2D). Further, gene  
405 set enrichment analysis (GSEA) revealed an upregulation of stress-response signatures in  
406 Ric<sup>EKO</sup> epidermis compared to control, including epidermal barrier stress response  
407 regulators (e.g. *Krt6a*, *Krt16*) <sup>39</sup> and UVB-induced genes in human epidermis (e.g.  
408 *S100a8*, *Tnfrsf10b*, *Il24*, *Mmp3*) (Figure 2D and E) <sup>40</sup>. Collectively, these findings reveal  
409 profound alterations in mTORC2 deficient epidermis in gene regulatory networks  
410 controlling terminal differentiation and barrier formation, and implicate a critical role for  
411 mTORC2 activity in the formation of a protective epidermal barrier.

412

### 413 **mTORC2 controls epidermal lipid metabolism**

414 Keratinocytes of the granular layer contribute to epidermal lipid synthesis which is  
415 essential for effective skin barrier function <sup>6, 41</sup>. During cornification, lipids are packed in  
416 intracellular lamellar bodies (LB) which then transport and release the lipids into the  
417 intercellular space of corneocytes to form a lipid bilayer. The lipid bilayer mainly  
418 consists of ceramides, cholesterol, and FFA <sup>6</sup>. To examine whether the structural and

419 functional SC defects in Ric<sup>EKO</sup> mice resulted from altered lipid composition, we further  
420 analyzed the SC lipid composition. Nile red, a fluorescent lipophilic dye, revealed that  
421 the lipid content was markedly diminished in Ric<sup>EKO</sup> SC (Figure 3A). To quantify SC  
422 lipid composition, the levels of ceramides, cholesterol, and FFA in the SC were  
423 determined using high performance thin layer chromatography (HPTLC). The analysis  
424 revealed a decrease of all three main SC lipid classes in Ric<sup>EKO</sup> epidermis. In particular,  
425 levels of Cer (NS) in Ric<sup>EKO</sup> epidermis were decreased by more than 40% compared to  
426 controls (Figure 3B).

427 Notably, consistent with the reduced SC lipid composition, the GSEA of RNA-seq data  
428 revealed a panel of lipid metabolism-associated genes which were significantly  
429 downregulated in Ric<sup>EKO</sup> epidermis. These genes include *Elovl3/4*, *Psap*, *Lipn*, *Pla2g3/5*,  
430 *Abhd5* (Figure 3C and D). Of note is that most of these genes have been shown to play a  
431 critical role in lipid metabolism and epidermal barrier formation in mice and patients with  
432 compromised skin barrier function<sup>42</sup>.

433 At the interface between the SG and SC, lipid lamellae are released into the intercellular  
434 space. We further examined the organization of LB. In line with the altered epidermal  
435 lipid composition, ultrastructural analysis by TEM revealed impaired lipid lamellae  
436 structure in the LB of Ric<sup>EKO</sup> epidermis. In addition, in Ric<sup>EKO</sup> epidermis, the lipid layer  
437 between SC and the SG was disrupted (Figure 3E). Taken together, these findings reveal  
438 multiple quantitative defects in SG lipid synthesis that lead to altered lipid composition  
439 and LB structure in mTORC2-deficient epidermis, potentially contributing to the  
440 compromised epidermal barrier function in Ric<sup>EKO</sup> mice.

441



442 **Reduced proteolytic activity is paralleled by impaired filaggrin processing in**  
443 **mTORC2 deficient epidermis**

444 Intriguingly, further pathway enrichment analysis using the KEGG database uncovered  
445 highly deregulated lysosomal transcripts in Ric<sup>EKO</sup> epidermis (Figure 4A). Genetic skin  
446 diseases and conditions with disturbed barrier function are often characterized by a  
447 disturbed balance of epidermal protease and antiprotease activities <sup>43</sup>. We thus  
448 hypothesized that attenuated proteolytic activity in Ric<sup>EKO</sup> epidermis might contribute to  
449 the disturbed barrier formation and function. Transcripts of several genes encoding  
450 members of diverse protease families, such as lysosomal cysteine, aspartic acid, and  
451 serine proteinases, were downregulated, including *cathepsin H (Ctsh)* and *cathepsin D*  
452 (*Ctsd*) (Figure 4B, C). Of interest is that *CTSH* and *CTSD* mutations have recently been  
453 shown to cause impaired filaggrin processing and disturbed SC formation <sup>26, 44</sup>.  
454 Conversely, Serpins, which encode potent protease inhibitors, were upregulated,  
455 including *Serpinb2*, which encodes an ovalbumin-like serine protease inhibitor and has  
456 been linked to the pathogenesis of certain cornification disorders <sup>45</sup> (Figure 4B, C).  
457 Moreover, expression of the gene encoding secretory leukocyte peptidase inhibitor (*Slpi*)  
458 was markedly increased in Ric<sup>EKO</sup> epidermis (Figure 4D). *Slpi* encodes an inhibitor of  
459 kallikrein 7, a protease required for corneodesmosome cleavage. Interestingly, TEM  
460 revealed that corneodesmosomes were retained in Ric<sup>EKO</sup> epidermis with an increase in  
461 both number and size (Figure 4E), thereby further corroborating an attenuated  
462 corneodesmosome degradation in the Ric<sup>EKO</sup> SC, potentially due to reduced Slpi.  
463 Further, proteolytic processing of the CE reinforcement protein profilaggrin is an  
464 essential process during proper keratinocyte terminal differentiation <sup>9</sup>. Having found that

465 *Ctsh* and *Ctsd*, encoding two proteases critically involved in profilaggrin processing, are  
466 downregulated in Ric<sup>EKO</sup> epidermis, we analyzed profilaggrin protein expression and  
467 processing in extracts prepared from control and Ric<sup>EKO</sup> epidermis by Western blot  
468 analysis. Notably, while filaggrin mRNA and profilaggrin protein expression levels were  
469 comparable between control and Ric<sup>EKO</sup> epidermis at P5, the level of filaggrin monomer  
470 was markedly reduced in mutant epidermis, suggesting that decreased epidermal protease  
471 activity might affect filaggrin processing in Ric<sup>EKO</sup> epidermis (Figure 4F and 4G).

472

### 473 **A keratinocyte-autonomous mTORC2-Akt axis controls filaggrin processing**

474 To tackle the molecular mechanism underlying decreased filaggrin processing in Ric<sup>EKO</sup>  
475 epidermis, we isolated primary keratinocytes from control and Ric<sup>EKO</sup> newborn mice and  
476 analyzed downstream targets of mTOR pathways during terminal differentiation triggered  
477 by Ca<sup>2+</sup> treatment<sup>46-47</sup>. Ca<sup>2+</sup> triggered activation of both mTORC1 (pS6-Ser240/244) and  
478 mTORC2 (pAkt-Ser473) in wild-type keratinocytes (Figure 5A). As expected, the  
479 absence of mTORC2 in Ric<sup>EKO</sup> keratinocytes abolished phosphorylation of Akt-Ser473 in  
480 response to Ca<sup>2+</sup> exposure (Figure 5A). Earlier studies had demonstrated that Akt is a  
481 critical regulator of profilaggrin processing during keratinocyte differentiation<sup>24-25</sup>.  
482 Notably, Western blot analysis revealed a pronounced reduction of processed trimer and  
483 monomer filaggrin in Ric<sup>EKO</sup> keratinocytes. Signals for other markers of keratinocyte  
484 differentiation, including loricrin and keratin 10 (K10), appeared unchanged in the  
485 knockout mice (Figure 5B).

486 To better define the role of mTORC2-mediated filaggrin processing, we retrovirally  
487 reconstituted Ric<sup>EKO</sup> keratinocytes with constitutively active myristoylated Akt1 (myr-

488 AKT)<sup>34</sup> and examined filaggrin processing. Empty pMSCV-IRES-GFP vector  
489 transfection served as control. Infection efficiencies were determined by analysis of  
490 IRES-driven GFP expression. GFP<sup>+</sup> cells were sorted by flow cytometry (FACS),  
491 expanded *in vitro*, and subjected to high Ca<sup>2+</sup>-induced differentiation. Western blot  
492 analysis confirmed abundant myr-AKT protein expression and increased Akt-Ser473  
493 phosphorylation signal in myr-AKT transduced keratinocytes (Figure 5C and D). In line  
494 with previous studies<sup>24-25</sup>, enforced myr-Akt expression increased filaggrin monomer  
495 expression in control keratinocytes upon calcium-triggered differentiation (Figure 5C).  
496 Importantly, restoration of Akt signaling in Ric<sup>EKO</sup> keratinocytes resulted in a significant  
497 increase in the amount of filaggrin monomer (Figure 5D), indicating that restored Akt-  
498 Ser473 phosphorylation enhanced filaggrin processing in Ric<sup>EKO</sup> cells. Taken together,  
499 our findings implicate mTORC2-mediated activation of Akt-Ser473 as a critical factor in  
500 effective filaggrin processing in keratinocyte terminal differentiation.

501

### 502 **Epidermal mTORC2 determines immune cell composition in the skin**

503 Epidermal barrier defects are often associated with altered immune responses and  
504 inflammatory skin diseases<sup>48</sup>. To assess the consequences of epidermal mTORC2-  
505 deficiency and the resulting barrier defect on the immune status, we examined  
506 inflammation mediator expression in prenatal E19.5 epidermis (RNA-seq analysis) and in  
507 P5 Ric<sup>EKO</sup> epidermis by qRT-PCR. Notably, whereas the RNA-seq analysis in prenatal  
508 E19.5 epidermis revealed downregulation of inflammation mediators when compared to  
509 controls (Figure 2B; Supplemental Table 3), postnatal (P5) expression of thymic stromal  
510 lymphopoietin (*Tslp*) and interleukin-24 (*Il24*) were markedly increased in Ric<sup>EKO</sup>

511 epidermis compared to littermate controls (Figure 6A). In contrast, transcripts for other  
512 potent inflammatory factors, including interleukin-1 $\alpha$  (*Il1a*), interleukin-1 $\beta$  (*Il1b*),  
513 interleukin-33 (*Il33*), chemokine ligand (*Ccl2*), and tumor necrosis factor- $\alpha$  (*Tnfa*), were  
514 not obviously altered in P5 Ric<sup>EKO</sup> epidermis (Figure 6A). To investigate further the  
515 impact of epidermal mTORC2 activity on cutaneous immune cell composition, we also  
516 performed immunohistochemical and fluorescent analyses in back skin of controls and  
517 Ric<sup>EKO</sup> mice at P5. While no major difference was detected in numbers of toluidine blue  
518 stained mast cells and dermal F4/80<sup>+</sup> macrophages, the number of dermal CD4<sup>+</sup> T cells  
519 was increased in Ric<sup>EKO</sup> mice (Figure 6B; Supplemental Figure 2A). The tendency  
520 towards an increase in CD4<sup>+</sup> cells in Ric<sup>EKO</sup> skin was corroborated by FACS analysis.  
521 Unexpectedly, these analyses further revealed that the percentage of CD3<sup>+</sup> $\gamma\delta$ -TCR<sup>+</sup> cells  
522 (Gate: 7-AAD<sup>-</sup>CD45<sup>+</sup>) was markedly reduced from 5.314 $\pm$ 0.708% to 0.350 $\pm$ 0.085% in  
523 Ric<sup>EKO</sup> skin (Figure 6C; Supplemental Figure 2B).

524 Dendritic epidermal T cells (DETCs) constitute a subset of T cells, which highly express  
525 the  $\gamma\delta$ -T cell receptor ( $\gamma\delta$ -TCR) and specifically localize to the epidermis<sup>49-50</sup>. Consistent  
526 with the FACS analysis, immunofluorescent staining for the pan-T cell marker CD3  
527 revealed a pronounced reduction of epidermal T cells in Ric<sup>EKO</sup> mice as compared to  
528 controls (Figure 7A). Further, epidermal CD3 and  $\gamma\delta$ -TCR co-staining revealed  
529 significantly reduced DETCs in Ric<sup>EKO</sup> epidermis (Figure 7A). Intriguingly, RNA-seq  
530 analysis of E19.5 Ric<sup>EKO</sup> epidermis revealed a significant downregulation of several  
531 members of the *Skint* family genes when compared to controls (Figure 7B).  $\gamma\delta$ -TCR  
532 ligand *Skint* genes are expressed by epidermal keratinocyte and play a critical role in  
533 maintaining the DETC pool in the epidermis and in regulating  $\gamma\delta$ -TCR cell homeostasis

534 <sup>51</sup>. Downregulated expression of *Skint1* and *Skint4* was confirmed by qRT-PCR analysis  
535 in control und mutant epidermis at P0 (Figure 7C).

536 To answer the question whether epidermal mTORC2 activity is important to maintain the  
537 homeostasis of DETCs throughout adulthood, we analyzed whole mounts from ear skin  
538 in adult mice at P70. Immunofluorescent analysis and FACS analysis revealed that the  
539 number of CD45<sup>+</sup>CD3e<sup>+</sup> $\gamma\delta$ -TCR<sup>high</sup>V $\gamma$ 3<sup>+</sup> DETCs was also markedly reduced in adult  
540 Ric<sup>EKO</sup> epidermal sheets, whereas the proportion of CD45<sup>+</sup>CD3e<sup>+</sup> $\gamma\delta$ -TCR<sup>low</sup>V $\gamma$ 3<sup>-</sup> dermal  
541  $\gamma\delta$  T cells was similar in Ric<sup>EKO</sup> mice and controls (Figure 7D, E; Supplemental Figure  
542 2C). Interestingly, the majority of DETCs in Ric<sup>EKO</sup> ears displayed an activated  
543 phenotype characterized by a rounded morphology and reduced dendritic spines as  
544 compared to DETCs in controls (Figure 7D). Reduced DETC number was paralleled by  
545 significantly reduced *Skint1* and *Skint4* transcripts (Figure 7F). Collectively, these  
546 findings reveal a critical role of epidermal mTORC2 activity in determining the  
547 composition of T cell subpopulations in naïve skin.

548

#### 549 **DNFB-mediated percutaneous immune response is enhanced in Ric<sup>EKO</sup> mice**

550 Barrier disruption and continuous percutaneous exposure to allergens presumably initiate  
551 and drive a variety of inflammatory skin diseases, including AD <sup>52</sup>. In fact, long-term  
552 observation under specific pathogen free (SPF) conditions revealed mildly dry eyes and  
553 perioral dermatitis in Ric<sup>EKO</sup> mice, to varying extent among individual mutants  
554 (Supplemental Figure 3A). Numbers of mast cells, CD4<sup>+</sup> T cells, and F4/80<sup>+</sup> myeloid  
555 cells and transcripts of proinflammatory mediators including *Il6*, *Tnfa*, *Il1 $\beta$* , and *Tslp*  
556 showed a tendency towards increase, yet, the difference did not reach statistical

557 significantly in unchallenged back skin of control and mutants at 10 weeks (Supplemental  
558 Figure 3B and C). In addition, although serum levels of circulating total IgE were  
559 increased in Ric<sup>EKO</sup> mice at 10 weeks, the difference did not reach statistical significance  
560 (Supplemental Figure 3D). To quantify the functional impact of epidermal mTORC2  
561 activity in percutaneous immune responses to exogenous substances, 10 week-old control  
562 and Ric<sup>EKO</sup> mice were subjected to established models of irritant (ICD) or allergic (ACD)  
563 contact dermatitis. Whereas no difference in ICD was observed between control and  
564 mutants (Supplemental Figure 3E), ACD in response to the hapten DNFB was  
565 significantly pronounced in mutants versus controls (Figure 8A). In controls the positive  
566 DNFB response was paralleled by a significant increase in epidermal phosphorylation of  
567 Akt-S473, an alteration of the cellular immune cell infiltrate with significant increase in  
568 numbers of F4/80<sup>+</sup> myeloid cells and a significant decline in DETCs (Figure 8C and  
569 Supplemental Figure 4). In contrast, the attenuated DNFB response in Ric<sup>EKO</sup> epidermis  
570 was associated with a significant reduction of epidermal Akt-S473 phosphorylation, an  
571 alteration of the cellular immune cell infiltrate with significant increase in numbers of  
572 granulocytes, F4/80<sup>+</sup> myeloid and CD4<sup>+</sup> T cells, and virtually absence of DETCs;  
573 differences in F4/80<sup>+</sup> myeloid cell, CD4<sup>+</sup> T cell and DETC cell infiltrate were  
574 significantly different in Ric<sup>EKO</sup> versus control mice (Figure 8C and Supplemental Figure  
575 4). In addition, transcripts of stress response genes including *Krt6b*, *S100a8* and *Spr2d*,  
576 and proinflammatory mediators such as *Il6*, *Tnfa* and *Il24*, were significantly increased in  
577 DNFB challenged ear skin in Ric<sup>EKO</sup> versus controls (Supplemental Figure 5).

578 Taken together, these findings strongly suggest that the impaired epidermal barrier in  
579 Ric<sup>EKO</sup> mice allows an increased hapten penetration, which in turn leads to the  
580 exaggerated stress and percutaneous immune responses.

581

Journal Pre-proof

582 **Discussion**

583 In the present study, we describe epidermal mTORC2 as central hub orchestrating the  
584 complex multicellular crosstalk and signaling required for postnatal epidermal barrier  
585 integrity and function. Specifically, we uncover a key role for epidermal mTORC2  
586 activity in the assembly of a protective SC (Figure 8D).

587 A prominent phenotype of Ric<sup>EKO</sup> mice is the dry, scaly, and ichthyosis-like appearance  
588 of skin. A similar phenotype is present in various mouse mutants and human skin  
589 diseases with epidermal barrier defects including ichthyosis, AD and multiple clinical  
590 eczema variants<sup>16, 53</sup>. Yet, an overarching mechanism that controls the multiple  
591 molecular factors in epidermal barrier formation is not resolved. Here, we propose the  
592 Ric<sup>EKO</sup> mouse as a novel preclinical disease model to advance our incomplete  
593 understanding of the molecular regulation of SC assembly and epidermal barrier function.  
594 Ric<sup>EKO</sup> mice displayed multiple skin symptoms which are also hallmarks in patients with  
595 compromised epidermal barrier function, including increased SC fragility and increased  
596 TEWL<sup>6</sup>. Ric<sup>EKO</sup> epidermis also showed dysbalanced protease/antiprotease activities  
597 combined with attenuated filaggrin processing, both previously reported to be associated  
598 with skin barrier defects in patients<sup>26, 44, 54-55</sup>. Thus, here we identified mTORC2 as a  
599 critical regulator of protease-mediated epidermal terminal differentiation.

600 In addition, a striking feature of *Rictor*-deficient epidermis is disturbed lipid composition.  
601 Specifically, we observed quantitative alterations in lipid content and structural  
602 alterations in lipid lamellae formation in Ric<sup>EKO</sup> epidermis. Consistently, expression of  
603 multiple genes previously reported to be essential in epidermal lipid synthesis and  
604 epidermal function in humans were reduced in Ric<sup>EKO</sup> epidermis emphasizing the utility



605 of Ric<sup>EKO</sup> mice as an attractive preclinical disease model for barrier defects<sup>10, 12-15</sup>.  
606 Recent reports describing a regulatory role for mTORC2 in *de novo* lipid synthesis are  
607 limited to hepatic and adipose tissues<sup>56-58</sup>. Here, we provide the first evidence of a role  
608 for mTORC2 in epidermal lipid metabolism. However, although it is widely accepted that  
609 epidermal lipids are integral components driving the formation and maintenance of the  
610 epidermal permeability barrier, the exact mechanistic link how epidermal lipids regulate  
611 epidermal barrier function and/or vice versa, is not entirely resolved<sup>59,60</sup>. Therefore,  
612 although our findings in Ric<sup>EKO</sup> mice suggest that the quantitative and qualitative  
613 perturbations in lipid composition is causative for the observed skin barrier defect in  
614 Ric<sup>EKO</sup> mice, at this stage we cannot exclude the possibility that perturbed epidermal  
615 architecture contributes to perturbed lipid synthesis<sup>59, 60</sup>. It will be of interest to  
616 investigate in future studies additional downstream mediators of mTORC2 signaling to  
617 understand how epidermal *de novo* lipogenesis and SC lipid homeostasis is regulated by  
618 mTORC2.

619 Intriguingly, the number of epidermal DETCs was remarkably reduced in Ric<sup>EKO</sup> mice.  
620 DETCs are profoundly reduced in patients with AD as well as in mouse models lacking  
621 key SC proteins<sup>30,61</sup>. Consistent with a reduced DETC number in Ric<sup>EKO</sup> epidermis, the  
622 expression of several members of *Skint* family genes was downregulated in Rictor-  
623 deficient epidermis. *Skint* genes have been identified as essential regulators of DETC cell  
624 development<sup>50</sup>. Hence, our findings indicate that epidermal mTORC2 activity is critical  
625 for anchoring DETCs in the epithelial niche and maintaining the DETC repertoire,  
626 potentially mediated via *Skint* genes. However, the reduced epidermal DETC number  
627 could be caused by a combination of multiple factors including attenuated expression of

628 *Skint* genes, perturbed epidermal architecture and/or disturbed interplay between lipids  
629 and/or additional factors and remains to be further investigated in future studies. In  
630 addition to the reduced number of epidermal DETCs, the morphology of DETCs was  
631 significantly altered in Ric<sup>EKO</sup> epidermis. DETCs in Ric<sup>EKO</sup> epidermal sheets lead to a  
632 phenotype associated with activation and a protective role in injured epidermis<sup>50</sup>. Thus, it  
633 is tempting to speculate that DETCs in Ric<sup>EKO</sup> epidermis compensate for a defective  
634 epidermal barrier. Together, our findings suggest an important function of epidermal  
635 mTORC2 in maintaining and shaping DETC homeostasis, and thus, highlight a  
636 previously unrecognized function of mTORC2 in the epithelial-immune crosstalk  
637 regulating skin barrier function. Along these lines, increased infiltration of CD4<sup>+</sup> T cells  
638 and enhanced expression of *Tslp* were also observed in the skin of Ric<sup>EKO</sup> pups, both of  
639 which are hallmarks in epidermis and keratinocytes of AD patients<sup>62</sup>. Although, the adult  
640 Ric<sup>EKO</sup> mouse skin displayed no spontaneous pathological phenotypes, including skin  
641 lesions or signs of skin inflammation, adult mutants exhibited exaggerated percutaneous  
642 immune responses. AD patients have an increased risk of sensitization to allergens, as  
643 well as asthma, rhinitis, and food allergy. Consistently, *FLG* deficiency in mice facilitates  
644 and permits increased percutaneous sensitization with protein allergens, irritants, and  
645 haptens<sup>63-64</sup>. Collectively, our findings highlight a direct link between epidermal  
646 mTORC2 deficiency and paradigmatic symptoms of patients with defective epidermal  
647 barrier conditions such as ichthyosis or AD.

648 An important question is what could be the mechanistic explanation for the various  
649 processes and symptoms observed in Ric<sup>EKO</sup> mice? A well-defined function of mTORC2  
650 is the phosphorylation of Akt at Ser473, which contributes to Akt-Thr308

651 phosphorylation by the phosphoinositide-dependent kinase 1 (PDK1), leading to full Akt  
652 activation<sup>20,65</sup>. Akt activity is elevated at the onset of keratinocyte differentiation and has  
653 been shown to regulate epidermal terminal differentiation<sup>18,24-25</sup>. However, the signaling  
654 events triggering epidermal Akt activation in epidermal differentiation still remain  
655 elusive. We propose a non-redundant role for mTORC2 in Akt-Ser473 activation during  
656 epidermal stratification and cornification. It is likely that epidermal mTORC2 acts  
657 through Akt in a PDK1-dependent manner since depletion of either component leads to  
658 an epidermal barrier phenotype comparable to that in Ric<sup>EKO</sup> mice<sup>66-67</sup>. Several *in vitro*  
659 and *in vivo* studies suggest that proper filaggrin processing requires Akt activation<sup>24-26</sup>.  
660 Accordingly, we observed that Akt-Ser473 phosphorylation was significantly attenuated  
661 and filaggrin processing was impaired in Ric<sup>EKO</sup> keratinocytes *in vitro*. Together, our  
662 findings suggest that the mTORC2-Akt signaling axis is activated and has mTORC1-  
663 independent functions upon terminal differentiation to trigger filaggrin processing and  
664 barrier function. Future studies are needed to determine whether induction of epidermal  
665 protease activity and/or lipid metabolism is a direct or indirect downstream target of  
666 mTORC2-Akt signaling.

667 Finally, prenatal Ric<sup>EKO</sup> epidermis presented a robust upregulation of a stress-response  
668 signature characterized by prominent expression of epidermal barrier stress-induced  
669 intermediate filament genes as well as UVB-induced genes. We hypothesize that this  
670 induced stress response supports a compensatory, protective mechanism in response to  
671 the barrier defect, thereby ensuring survival. This hypothesis is further based on the  
672 finding that the cytoprotective transcription factor *Nrf2* and several well known Nrf2-  
673 target genes, including *Krt6*, *Krt16*, *Sprr2h*, and *S100a* were all transcriptionally

674 upregulated in Ric<sup>EKO</sup> epidermis <sup>68</sup>. Along these lines, a Nrf2-regulated compensatory  
675 response has been shown to be activated in embryonic epidermis lacking loricrin <sup>69</sup>.  
676 Therefore, our findings support the idea that the activation of a stress-related homeostatis  
677 program is a general feature of a functionally compromised epidermal barrier. Our  
678 discovery that the druggable mTORC2 complex orchestrates this generalized stress  
679 response opens interesting avenues for exploring therapeutic boosting of barrier function.  
680 In conclusion, we have demonstrated that postnatal epidermal mTORC2 activity  
681 orchestrates epidermal barrier formation and maintenance via regulation of lipid synthesis  
682 and filaggrin processing. We speculate that altered mTORC2 activity may represent  
683 another predisposing factor for skin disorders associated with disrupted barrier function.  
684 Our findings might be of clinical relevance by, for example, normalizing epidermal  
685 mTORC2 activity in patients with defective epidermal barrier conditions by  
686 pharmacotherapy.

687

688 **Author Contributions**

689 XD and SAE conceptualized the study, performed experiments, analyzed the data, and  
690 drafted the manuscript; WB performed TEM analysis; SW helped with flow cytometry  
691 and experimental animal work; PW performed the bio-informatic analyses; SB performed  
692 the lipid analysis; MNH and MAR provided *Rictor* floxed mouse lines; AJ, JCB, SAW,  
693 AR, MNH, MAR have made substantial contributions to the analysis and interpretation of  
694 data and critical revising of the drafted manuscript.

695

696 **Acknowledgments**

697 We thank Michael Piekarek, Gabriele Scherr, and Sebastian Wüst for excellent technical  
698 assistance. The authors thank Dr. Stephen M. Sykes (Fox Chase Cancer Center,  
699 Philadelphia) and Dr. Kira Gritsman (Department of Medicine, Albert Einstein College of  
700 Medicine) for the gift of the myr-AKT plasmid used in this study; we thank Dr. Sandra  
701 Iden for providing antibodies. We thank Dr. Carien Niessen and colleagues in her group  
702 for insightful suggestions and technical advice in TEWL measurements. We thank Dr.  
703 Peter Nürnberg and Dr. Janine Altmüller (Cologne Center for Genomics, University of  
704 Cologne, Germany) for supporting transcriptome and bioinformatic analyses. We also  
705 thank the Imaging Facility (CECAD, Cologne University) and Dr. Gunter Rappl, (Central  
706 Cell Sorting Facility, CMMC, Cologne University) for specialized technical support. The  
707 funding source for this manuscript was the Deutsche Forschungsgemeinschaft (SAE,  
708 SAW, JCB to Projektnummer 73111208 - SFB829 and CECAD), (SAE, AR to  
709 FOR2599), and the Center for Molecular Medicine (SAE).

710

711 **References**

- 712 1. Elias PM. Skin barrier function. *Curr Allergy and Asthma Rep* 2008; 8:299-305.
- 713 2. Kubo A, Nagao K, Amagai M. Epidermal barrier dysfunction and cutaneous  
714 sensitization in atopic diseases. *J Clin Invest* 2012; 122:440-447.
- 715 3. Duff M, Demidova O, Blackburn S, Shubrook J. Cutaneous manifestations of  
716 diabetes mellitus. *Clin Diabetes* 2015; 33:40-48.
- 717 4. Boireau-Adamezyk E, Baillet-Guffroy A, Stamatatos GN. Age-dependent changes  
718 in stratum corneum barrier function. *Skin Res Technol* 2014; 20:409-415.
- 719 5. Craiglow BG. Ichthyosis in the newborn. *Semin in Perinatol* 2013; 37:26-31.
- 720 6. Candi E, Schmidt R, Melino G. The cornified envelope: a model of cell death in  
721 the skin. *Nat Rev Mol Cell Biol* 2005; 6:328-340.
- 722 7. Lopez-Pajares V, Yan K, Zarnegar BJ, Jameson KL, Khavari PA. Genetic  
723 pathways in disorders of epidermal differentiation. *Trends Genet* 2013; 29:31-40.
- 724 8. Smith FJD, Irvine AD, Terron-Kwiatkowski A, Sandilands A, Campbell LE, Zhao  
725 YW, et al. Loss-of-function mutations in the gene encoding filaggrin cause  
726 ichthyosis vulgaris. *Nat Genet* 2006; 38:337-342.
- 727 9. Sandilands A, Sutherland C, Irvine AD, McLean WH. Filaggrin in the frontline:  
728 role in skin barrier function and disease. *J Cell Sci* 2009; 122:1285-1294.
- 729 10. Brunner PM, Israel A, Zhang N, Leonard A, Wen HC, Huynh T, et al. Early-onset  
730 pediatric atopic dermatitis is characterized by T(H)2/T(H)17/T(H)22-centered  
731 inflammation and lipid alterations. *J Allergy Clin Immunol* 2018; 141:2094-2106.

- 732 11. Gruber R, Elias PM, Crumrine D, Lin TK, Brandner JM, Hachem JP, et al.  
733 Filaggrin Genotype in Ichthyosis Vulgaris Predicts Abnormalities in Epidermal  
734 Structure and Function. *Am J Pathol* 2011; 178:2252-2263.
- 735 12. Vasireddy V, Uchida Y, Salem N, Kim SY, Mandal MNA, Reddy GB, et al. Loss  
736 of functional ELOVL4 depletes very long-chain fatty acids ( $\geq$  C28) and the  
737 unique omega-O-acylceramides in skin leading to neonatal death. *Hum Mol Genet*  
738 2007; 16:471-482.
- 739 13. Westerberg R, Tvrdik P, Uden AB, Mansson JE, Norlen L, Jakobsson A, et al.  
740 Role for ELOVL3 and fatty acid chain length in development of hair and skin  
741 function. *J Biol Chem* 2004; 279:5621-5629.
- 742 14. Aldahmesh MA, Mohamed JY, Alkuraya HS, Verma IC, Puri RD, Alaiya AA, et  
743 al. Recessive mutations in ELOVL4 cause ichthyosis, intellectual disability, and  
744 spastic quadriplegia. *Am J Hum Genet* 2011; 89:745-750.
- 745 15. Ilic D, Bollinger JM, Gelb M, Mauro TM. sPLA2 and the epidermal barrier.  
746 *Biochim Biophys Acta* 2014; 1841:416-421.
- 747 16. Natsuga K. Epidermal Barriers. *Cold Spring Harb Perspect Med* 2014; 4:a018218.
- 748 17. Blanpain C, Fuchs E. Epidermal homeostasis: a balancing act of stem cells in the  
749 skin. *Nat Rev Mol Cell Biol* 2009; 10:207-217.
- 750 18. Ding X, Bloch W, Iden S, Ruegg MA, Hall MN, Leptin M, et al. mTORC1 and  
751 mTORC2 regulate skin morphogenesis and epidermal barrier formation. *Nat*  
752 *Commun* 2016; 7:13226.

- 753 19. Kakanj P, Moussian B, Gronke S, Bustos V, Eming SA, Partridge L, et al. Insulin  
754 and TOR signal in parallel through FOXO and S6K to promote epithelial wound  
755 healing. *Nat Commun* 2016; 7:12972.
- 756 20. Saxton RA, Sabatini DM. mTOR Signaling in Growth, Metabolism, and Disease.  
757 *Cell* 2017; 168:960-976.
- 758 21. Wullschleger S, Loewith R, Hall MN. TOR signaling in growth and metabolism.  
759 *Cell* 2006; 124:471-484.
- 760 22. Sarbassov DD, Ali SM, Sengupta S, Sheen JH, Hsu PP, Bagley AF, et al.  
761 Prolonged rapamycin treatment inhibits mTORC2 assembly and Akt/PKB. *Mol*  
762 *Cell* 2006; 22:159-168.
- 763 23. Jacinto E, Loewith R, Schmidt A, Lin S, Ruegg MA, Hall A, et al. Mammalian  
764 TOR complex 2 controls the actin cytoskeleton and is rapamycin insensitive. *Nat*  
765 *Cell Biol* 2004; 6:1122-1128.
- 766 24. Calautti E, Li J, Saoncella S, Brissette JL, Goetinck PF. Phosphoinositide 3-  
767 kinase signaling to Akt promotes keratinocyte differentiation versus death. *J Biol*  
768 *Chem* 2005; 280:32856-32865.
- 769 25. O'Shaughnessy RF, Welte JC, Cooke JC, Avilion AA, Monks B, Birnbaum MJ, et  
770 al. AKT-dependent HspB1 (Hsp27) activity in epidermal differentiation. *J Biol*  
771 *Chem* 2007; 282:17297-17305.
- 772 26. Naeem AS, Tommasi C, Cole C, Brown SJ, Zhu Y, Way B, et al. A mechanistic  
773 target of rapamycin complex 1/2 (mTORC1)/V-Akt murine thymoma viral  
774 oncogene homolog 1 (AKT1)/cathepsin H axis controls filaggrin expression and



- 775 processing in skin, a novel mechanism for skin barrier disruption in patients with  
776 atopic dermatitis. *J Allergy Clin Immunol* 2016; 139:1228-1241.
- 777 27. Ding X, Lucas T, Marcuzzi GP, Pfister H, Eming SA. Distinct functions of  
778 epidermal and myeloid-derived VEGF-A in skin tumorigenesis mediated by  
779 HPV8. *Cancer Res* 2015; 75:330-343.
- 780 28. Knipper JA, Willenborg S, Brinckmann J, Bloch W, Maass T, Wagener R, et al.  
781 Interleukin-4 Receptor alpha Signaling in Myeloid Cells Controls Collagen Fibril  
782 Assembly in Skin Repair. *Immunity* 2015; 43:803-816.
- 783 29. Subramanian A, Tamayo P, Mootha VK, Mukherjee S, Ebert BL, Gillette MA, et  
784 al. Gene set enrichment analysis: a knowledge-based approach for interpreting  
785 genome-wide expression profiles. *Proc Natl Acad Sci U S A* 2005; 102:15545-  
786 15550.
- 787 30. Sevilla LM, Nachat R, Groot KR, Klement JF, Uitto J, Djian P, et al. Mice  
788 deficient in involucrin, envoplakin, and periplakin have a defective epidermal  
789 barrier. *J Cell Biol* 2007; 179:1599-1612.
- 790 31. Reichelt J, Breiden B, Sandhoff K, Magin TM. Loss of keratin 10 is accompanied  
791 by increased sebocyte proliferation and differentiation. *Eur J Cell Biol* 2004;  
792 83:747-759.
- 793 32. Signorelli P, Hannun YA. Analysis and quantitation of ceramide. *Methods*  
794 *Enzymol* 2002; 345:275-294.
- 795 33. Belgardt BF, Mauer J, Wunderlich FT, Ernst MB, Pal M, Spohn G, et al.  
796 Hypothalamic and pituitary c-Jun N-terminal kinase 1 signaling coordinately  
797 regulates glucose metabolism. *Proc Natl Acad Sci U S A* 2010; 107:6028-6033.

- 798 34. Kharas MG, Okabe R, Ganis JJ, Gozo M, Khandan T, Paktinat M, et al.  
799 Constitutively active AKT depletes hematopoietic stem cells and induces  
800 leukemia in mice. *Blood* 2010; 115:1406-1415.
- 801 35. Ding X, Wang X, Sontag S, Qin J, Wanek P, Lin Q, et al. The polycomb protein  
802 Ezh2 impacts on induced pluripotent stem cell generation. *Stem Cells Dev* 2014;  
803 23:931-940.
- 804 36. Bentzinger CF, Romanino K, Cloetta D, Lin S, Mascarenhas JB, Oliveri F, et al.  
805 Skeletal Muscle-Specific Ablation of raptor, but Not of rictor, Causes Metabolic  
806 Changes and Results in Muscle Dystrophy. *Cell Metab* 2008; 8:411-424.
- 807 37. Hafner M, Wenk J, Nenci A, Pasparakis M, Scharffetter-Kochanek K, Smyth N,  
808 et al. Keratin 14 Cre transgenic mice authenticate keratin 14 as an oocyte-  
809 expressed protein. *Genesis* 2004; 38:176-181.
- 810 38. Mischke D, Korge BP, Marenholz I, Volz A, Ziegler A. Genes encoding structural  
811 proteins of epidermal cornification and S100 calcium-binding proteins form a  
812 gene complex ("epidermal differentiation complex") on human chromosome 1q21.  
813 *J Invest Dermatol* 1996; 106:989-992.
- 814 39. Lessard JC, Pina-Paz S, Rotty JD, Hickerson RP, Kaspar RL, Balmain A, et al.  
815 Keratin 16 regulates innate immunity in response to epidermal barrier breach.  
816 *Proc Natl Acad Sci U S A* 2013; 110:19537-19542.
- 817 40. Enk CD, Jacob-Hirsch J, Gal H, Verbovetski I, Amariglio N, Mevorach D, et al.  
818 The UVB-induced gene expression profile of human epidermis in vivo is different  
819 from that of cultured keratinocytes. *Oncogene* 2006; 25:2601-2614.

- 820 41. Elias PM, Williams ML, Holleran WM, Jiang YJ, Schmuth M. Pathogenesis of  
821 permeability barrier abnormalities in the ichthyoses: inherited disorders of lipid  
822 metabolism. *J Lipid Res* 2008; 49:697-714.
- 823 42. Breiden B, Sandhoff K. The role of sphingolipid metabolism in cutaneous  
824 permeability barrier formation. *Biochim Biophys Acta* 2014; 1841:441-452.
- 825 43. Ovaere P, Lippens S, Vandenabeele P, Declercq W. The emerging roles of serine  
826 protease cascades in the epidermis. *Trends Biochem Sci* 2009; 34:453-463.
- 827 44. Egberts F, Heinrich M, Jensen JM, Winoto-Morbach S, Pfeiffer S, Wickel M, et al.  
828 Cathepsin D is involved in the regulation of transglutaminase 1 and epidermal  
829 differentiation. *J Cell Sci* 2004; 117:2295-2307.
- 830 45. Oji V, Oji ME, Adamini N, Walker T, Aufenvenne K, Raghunath M, et al.  
831 Plasminogen activator inhibitor-2 is expressed in different types of congenital  
832 ichthyosis: in vivo evidence for its cross-linking into the cornified cell envelope  
833 by transglutaminase-1. *Br J Dermatol* 2006; 154:860-867.
- 834 46. Yuspa SH, Kilkenny AE, Steinert PM, Roop DR. Expression of murine epidermal  
835 differentiation markers is tightly regulated by restricted extracellular calcium  
836 concentrations in vitro. *J Cell Biol* 1989; 109:1207-1217.
- 837 47. Tu CL, Crumrine DA, Man MQ, Chang WH, Elalieh H, You M, et al. Ablation of  
838 the Calcium-Sensing Receptor in Keratinocytes Impairs Epidermal Differentiation  
839 and Barrier Function. *J Invest Dermatol* 2012; 132:2350-2359.
- 840 48. Elias PM. Therapeutic Implications of a Barrier-based Pathogenesis of Atopic  
841 Dermatitis. *Ann Dermatol* 2010; 22:245-254.

- 842 49. Komori H, Meehar TF, Havran WL. Epithelial and mucosal gamma delta T cells.  
843 Curr Opin in Immunol 2006; 18:534-538.
- 844 50. Nielsen MM, Witherden DA, Havran WL.  $\gamma\delta$  T cells in homeostasis and host  
845 defence of epithelial barrier tissues. Nat Rev Immunol 2017; 17:733-745.
- 846 51. Barbee SD, Woodward MJ, Turchinovich G, Mention JJ, Lewis JM, Boyden LM,  
847 et al. Skint-1 is a highly specific, unique selecting component for epidermal T  
848 cells. Proc Natl Acad Sci U S A 2011; 108:3330-3335.
- 849 52. De Benedetto A, Kubo A, Beck LA. Skin barrier disruption: a requirement for  
850 allergen sensitization? J Invest Dermatol 2012; 132:949-963.
- 851 53. Weidinger S, Novak N. Atopic dermatitis. Lancet 2016; 387:1109–22.
- 852 54. Toomes C, James J, Wood AJ, Wu CL, McCormick D, Lench N, et al. Loss-of-  
853 function mutations in the cathepsin C gene result in periodontal disease and  
854 palmoplantar keratosis. Nat Genet 1999; 23:421-424.
- 855 55. Cheng T, Hitomi K, van Vlijmen-Willems IMJJ, de Jongh GJ, Yamamoto K,  
856 Nishi K, et al. Cystatin M/E is a high affinity inhibitor of cathepsin V and  
857 cathepsin L by a reactive site that is distinct from the legumain-binding site - A  
858 novel clue for the role of cystatin M/E in epidermal cornification. J Biol Chem  
859 2006; 281:15893-15899.
- 860 56. Caron A, Richard D, Laplante M. The Roles of mTOR Complexes in Lipid  
861 Metabolism. Annu Rev Nutr 2015; 35:321-348.
- 862 57. Guri Y, Colombi M, Dazert E, Hindupur SK, Roszik J, Moes S, et al. mTORC2  
863 Promotes Tumorigenesis via Lipid Synthesis. Cancer Cell 2017; 32:807-823.

- 864 58. Hagiwara A, Cornu M, Cybulski N, Polak P, Betz C, Trapani F, et al. Hepatic  
865 mTORC2 Activates Glycolysis and Lipogenesis through Akt, Glucokinase, and  
866 SREBP1c. *Cell Metab* 2012; 15:725-738.
- 867 59. van Smeden J, Janssens M, Gooris GS, Bouwstra JA. The important role of stratum  
868 corneum lipids for the cutaneous barrier function. *Biochim Biophys Acta* 2014;  
869 1841:295-313.
- 870 60. Bhattacharya N, Sato WJ, Kelly A, Ganguli-Indra G, Indra AK. Epidermal lipids:  
871 key mediators of atopic dermatitis pathogenesis. *Trends Mol Med* doi:  
872 10.1016/j.molmed.2019.04.001 [Epub ahead of print May 01, 2019].
- 873 61. Katsuta M, Takigawa Y, Kimishima M, Inaoka M, Takahashi R, Shiohara T. NK  
874 cells and gamma delta(+) T cells are phenotypically and functionally defective  
875 due to preferential apoptosis in patients with atopic dermatitis. *J Immunol* 2006;  
876 176:7736-7744.
- 877 62. Ziegler SF, Artis D. Sensing the outside world: TSLP regulates barrier immunity.  
878 *Nat Immunol* 2010; 11:289-293.
- 879 63. Kawasaki H, Nagao K, Kubo A, Hata T, Shimizu A, Mizuno H, et al. Altered  
880 stratum corneum barrier and enhanced percutaneous immune responses in  
881 filaggrin-null mice. *J Allergy Clin Immunol* 2012; 129:1538-1546.
- 882 64. Fallon PG, Sasaki T, Sandilands A, Campbell LE, Saunders SP, Mangan NE, et al.  
883 A homozygous frameshift mutation in the mouse Flg gene facilitates enhanced  
884 percutaneous allergen priming. *Nat Genet* 2009; 41:602-608.

- 885 65. Sarbassov DD, Guertin DA, Ali SM, Sabatini DM. Phosphorylation and  
886 regulation of Akt/PKB by the rictor-mTOR complex. *Science* 2005; 307:1098-  
887 1101.
- 888 66. Dainichi T, Hayden MS, Park SG, Oh H, Seeley JJ, Grinberg-Bleyer Y, et al.  
889 PDK1 Is a Regulator of Epidermal Differentiation that Activates and Organizes  
890 Asymmetric Cell Division. *Cell Rep* 2016; 15:1615-1623.
- 891 67. Peng XD, Xu PZ, Chen ML, Hahn-Windgassen A, Skeen J, Jacobs J, et al.  
892 Dwarfism, impaired skin development, skeletal muscle atrophy, delayed bone  
893 development, and impeded adipogenesis in mice lacking Akt1 and Akt2. *Genes*  
894 *Dev* 2003; 17:1352-1365.
- 895 68. Schafer M, Farwanah H, Willrodt AH, Huebner AJ, Sandhoff K, Roop D, et al.  
896 Nrf2 links epidermal barrier function with antioxidant defense. *EMBO Mol Med*  
897 2012; 4:364-379.
- 898 69. Huebner AJ, Dai D, Morasso M, Schmidt EE, Schafer M, Werner S, et al.  
899 Amniotic fluid activates the nrf2/keap1 pathway to repair an epidermal barrier  
900 defect in utero. *Dev Cell* 2012; 23:1238-1246.
- 901
- 902

903 **Figure legends**904 **Figure 1. Ric<sup>EKO</sup> mice display a transient ichthyosis-like phenotype.**

905 (A) Western blot analysis in epidermal isolates at P5. (B) Macroscopic appearance of  
906 littermates; boxed areas are shown at higher magnifications. (C) HE-stained back skin  
907 sections at P4 and quantification of epidermal thickness; e, epidermis; d, dermis; SC,  
908 stratum corneum; white dashed line indicates basal membrane, scale bar, 25  $\mu$ m. (D)  
909 Quantification of TEWL at P4, each dot or square represents one mouse. (E) Body weight  
910 at P5. (F) Left: micrographs of isolated CE from back skin at P4. Right: quantification of  
911 the intact CE, each dot or square represents isolates from one mouse. (G) TEM image  
912 shows poorly condensed SC in Ric<sup>EKO</sup> mice, note the presence of cell organelles in C1 of  
913 Ric<sup>EKO</sup> mice (indicated by arrow). SG, stratum granulosum; C1, cornified layer 1, scale  
914 bar, 0.5  $\mu$ m. Data are expressed as the mean; unpaired t-test was used to calculate *P* value;  
915 \*\**P* < 0.01; \*\*\**P* < 0.001.

916

917 **Figure 2. Epidermal mTORC2 deficiency induces a compensatory transcriptional**  
918 **epidermal repair program in Ric<sup>EKO</sup> mice.**

919 (A) Volcano plot of differentially regulated transcripts between control and Ric<sup>EKO</sup>  
920 epidermis at E19.5 (*n*=3 per genotype). Colored data points meet the thresholds of a log<sub>2</sub>  
921 fold change of higher than 1 or lower than -1 and an adjusted *P* value of lower than 0.05.  
922 (B) GO of differentially regulated transcripts from Ric<sup>EKO</sup> vs. control comparison using  
923 DAVID 6.8 online software. Only genes that have fold change >1.5 and a *P* value < 0.05  
924 were used. (C) Log<sub>2</sub> fold changes of EDC gene expression in the epidermis of Ric<sup>EKO</sup>  
925 skin. EDC genes with an alteration of fold change > 2 and *P* value < 0.05 are shown.

926 (D) qRT-PCR analysis validation of differentially expressed genes from RNA-seq data in  
927 P0 epidermis ( $n=5$ /genotype). (E) Left: epidermal UV-response gene set enrichment plot  
928 in Ric<sup>EKO</sup> samples. Right: heat map shows the stress-response genes with positive  
929 enrichment in Ric<sup>EKO</sup> samples. All data are presented as mean  $\pm$  s.e.m; unpaired t-test was  
930 used to calculate the  $P$  value; \* $P < 0.05$ ; \*\* $P < 0.01$ ; \*\*\* $P < 0.001$ .

931

932 **Figure 3. mTORC2 controls epidermal lipid metabolism.**

933 (A) Fluorescent dye Nile red staining and quantification of back skin sections at P1( $n=4$ );  
934 counterstained with DAPI; e, epidermis; d, dermis; white dashed line indicates basal  
935 membrane; scale bar, 25  $\mu$ m. (B) Analysis of SC lipids by HPTLC ( $n=3$  per genotype).  
936 Cer, ceramide; FFA, free fatty acid; Chol, cholesterol. (C) Left: GSEA of differentially  
937 regulated genes between control and Ric<sup>EKO</sup> epidermis identifies enrichment of lipid and  
938 lipoprotein metabolism genes. Right: hierarchically clustered heat map illustration shows  
939 differential expression of lipid metabolism-related genes from RNA-seq data. (D) qRT-  
940 PCR analysis of *Elovl3* and *Pla2g5* in epidermis at P0 ( $n=5$  per genotype). (E)  
941 Ultrastructural analysis of the interface between SG and SC at P5. Ric<sup>EKO</sup> epidermis  
942 shows a disorganized interface (red arrows) between SG and SC, and displayed LB  
943 abnormalities, including disoriented lamellae and reduced lamellae number. In contrast,  
944 the LB of control showed regular lamellae orientation with equal distances lamellae (red  
945 bars). SG, stratum granulosum; C1, cornified layer 1; C2, cornified layer 2; LB, lamellar  
946 body, scale bar, 200 nm. All data are presented as mean  $\pm$  s.e.m; unpaired t-test was used  
947 to calculate the  $P$  value; \* $P < 0.05$ ; \*\* $P < 0.01$ ; \*\*\* $P < 0.001$ .

948



949 **Figure 4. Reduced proteolytic activity and impaired filaggrin processing in Ric<sup>EKO</sup>**  
950 **epidermis.**

951 (A) GSEA of RNA-seq data identifies enrichment of the (KEGG) lysosome gene set. (B)  
952 Hierarchically clustered heat map shows altered expression of protease and protease  
953 inhibitor genes. (C) qRT-PCR analysis of indicated genes at P0 ( $n=5$ ). (D) qRT-PCR  
954 analysis shows downregulated *Slpi* expression in Ric<sup>EKO</sup> epidermis ( $n=5$ ). (E) TEM  
955 analysis shows delayed corneodesmosome degradation in Ric<sup>EKO</sup> epidermis at P5.  
956 Corneocyte layers (C) were numbered, arrows point to corneodesmosomes. SG, stratum  
957 granulosum; scale bar, 200nm. (F) qRT-PCR analysis of epidermal filaggrin mRNA  
958 expression at P5 ( $n=5$ ). (G) Left, Western blot analysis at P5; Profilaggrin (Pro-FLG),  
959 trimer (3F), dimer (2F) and monomer (1F) filaggrin are indicated. Right, quantified ratio  
960 of filaggrin monomer (1F) and total filaggrin, Pro-filaggrin and  $\beta$ -actin with control set to  
961 1 ( $n=4$ ). All data are presented as mean  $\pm$  s.e.m; unpaired t-test was used to calculate the  
962 P value; \* $P < 0.05$ ; \*\* $P < 0.01$ ; \*\*\* $P < 0.001$ .

963

964 **Figure 5. A keratinocyte-autonomous mTORC2-Akt axis controls filaggrin**  
965 **processing.**

966 (A) Western blot analysis in cultured control and Ric<sup>EKO</sup> keratinocytes, stimulated by  
967 high concentration Ca<sup>2+</sup> (0.2 mM). (B) Left, representative Western blot analysis in  
968 keratinocytes; right, graph of relative densitometry of filaggrin trimer (3F), dimer (2F)  
969 and monomer (1F). (C) Western blot analysis of filaggrin and Akt protein expression in  
970 empty vector (control) and myr-Akt retrovirus infected control keratinocytes. (D) Left,  
971 Western blot analysis in empty vector (control) and myr-Akt retrovirus infected Ric<sup>EKO</sup>

972 keratinocytes; right, graph of relative densitometry of filaggrin trimer (3F), dimer (2F)  
973 and monomer (1F). All data are presented as mean  $\pm$  s.e.m; unpaired t-test was used to  
974 calculate the *P* value; \**P* < 0.05; \*\**P* < 0.01.

975

976 **Figure 6. Epidermal mTORC2 determines immune cell composition in the skin.**

977 (A) qRT-PCR profile in epidermis at P5 (*n*=8 per genotype). (B) Left: CD4  
978 immunostaining on back skin sections at P5. Right: quantification of CD4<sup>+</sup> cells at high-  
979 power field (HPF). e, epidermis; d, dermis; white dashed line indicates basal membrane;  
980 scale bar, 25  $\mu$ m. (C) Left: flow cytometry profile of  $\gamma\delta$ -TCR<sup>+</sup> CD3<sup>+</sup> cells at P5; right,  
981 percentage of different cell populations are shown at P5 (*n*=6 per genotype); cells were  
982 gated on 7-AAD<sup>-</sup> CD45<sup>+</sup> skin cells. All data are presented as mean  $\pm$  s.e.m; unpaired t-  
983 test was used to calculate the *P* value; \**P* < 0.05; \*\**P* < 0.01; \*\*\**P* < 0.001.

984

985 **Figure 7. DETC number is reduced in Ric<sup>EKO</sup> epidermis.**

986 (A) Left: CD3 and  $\gamma\delta$ -TCR immunostaining on back skin at P5; Right: quantification of  
987 epidermal CD3<sup>+</sup> and  $\gamma\delta$ -TCR<sup>+</sup> cells per 500  $\mu$ m of basement membrane; white dashed  
988 line indicates basal membrane; scale bar, 25  $\mu$ m. (B) Hierarchically clustered heat map  
989 shows altered expression of *skint* family genes in Ric<sup>EKO</sup> epidermis from RNA-seq data.  
990 (C) qRT-PCR analysis validates reduced *Skint1* and *Skint4* expression in Ric<sup>EKO</sup>  
991 epidermis at P0 (*n*=5 per genotype). (D) Left: DETCs in epidermis of ear sheet at P70;  
992 separated epidermis was stained against  $\gamma\delta$ -TCR. Right: quantification of  $\gamma\delta$ -TCR<sup>+</sup> cells  
993 in the epidermal sheets. Scale bar, 25  $\mu$ m. (E) Left: flow cytometry profile of single cell  
994 suspensions of ear skin at P70. 7-AAD<sup>-</sup>CD45<sup>+</sup>CD3e<sup>+</sup> cells were gated and analyzed for

995 expression of  $\gamma\delta$ -TCR and V $\gamma$ 3-TCR, (right) quantification of  $\gamma\delta$ -TCR<sup>low</sup>V $\gamma$ 3-TCR<sup>-</sup>  
996 dermal  $\gamma\delta$  T cells and  $\gamma\delta$ -TCR<sup>high</sup>V $\gamma$ 3-TCR<sup>+</sup> DETCs. (F) qRT-PCR analysis of *Skint1* and  
997 *Skint4* expression in adult epidermis at P70 ( $n=5$  per genotype). Each dot or square  
998 represents one mouse. Data are presented as mean or as mean  $\pm$  s.e.m; unpaired t-test was  
999 used to calculate the  $P$  value; \* $P < 0.05$ ; \*\* $P < 0.01$ ; \*\*\* $P < 0.001$ .

1000

1001 **Figure 8. Enhanced percutaneous immune response in Ric<sup>EKO</sup> mice.**

1002 (A) DNFB-induced ACD response; right, H&E-staining of DNFB-treated ears. e,  
1003 epidermis; d, dermis; c, cartilage, \* $P < 0.05$ ; \*\*\* $P < 0.001$ . (B) pAkt-S473  
1004 immunofluorescent staining and morphometric quantification of pAkt-S473 stained  
1005 unchallenged (0 h) and challenged (48 h) ear skin sections. (C) The number of  
1006 eosinophils (Siglec F), mast cells (Giemsa), neutrophils (Gr1), macrophages (F4/80) and  
1007 T cells (CD4 and  $\gamma\delta$ -TCR) per high power field (HPF, 400x) in unchallenged (0 h) and  
1008 challenged ear (48 h) ear tissues. (D) Schematic diagram illustrating the proposed  
1009 function of mTORC2 in regulating epidermal barrier function. Each dot or square  
1010 represents one mouse. Data are presented as mean or as mean  $\pm$  s.e.m; unpaired t-test or  
1011 ANOVA one-way test analysis with Bonferroni multiple comparison test was used to  
1012 calculate the  $P$  value; \* $P < 0.05$ ; \*\* $P < 0.01$ ; \*\*\* $P < 0.001$ .

1013

Figure 1

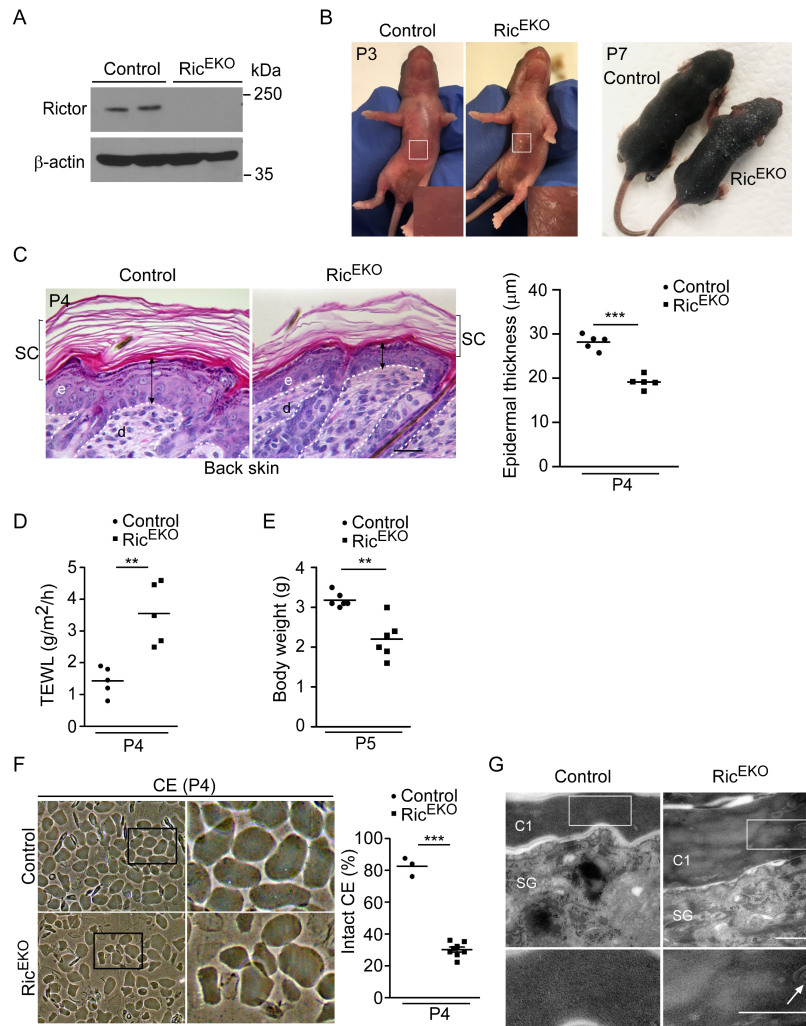


Figure 2

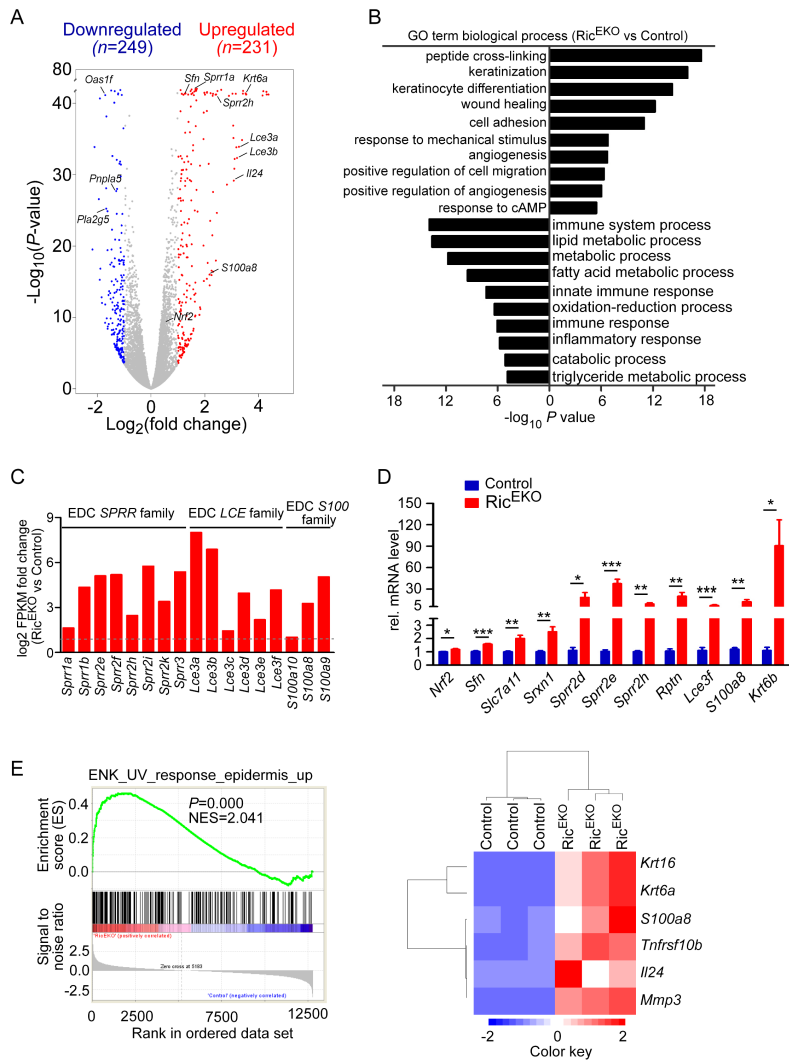


Figure 3

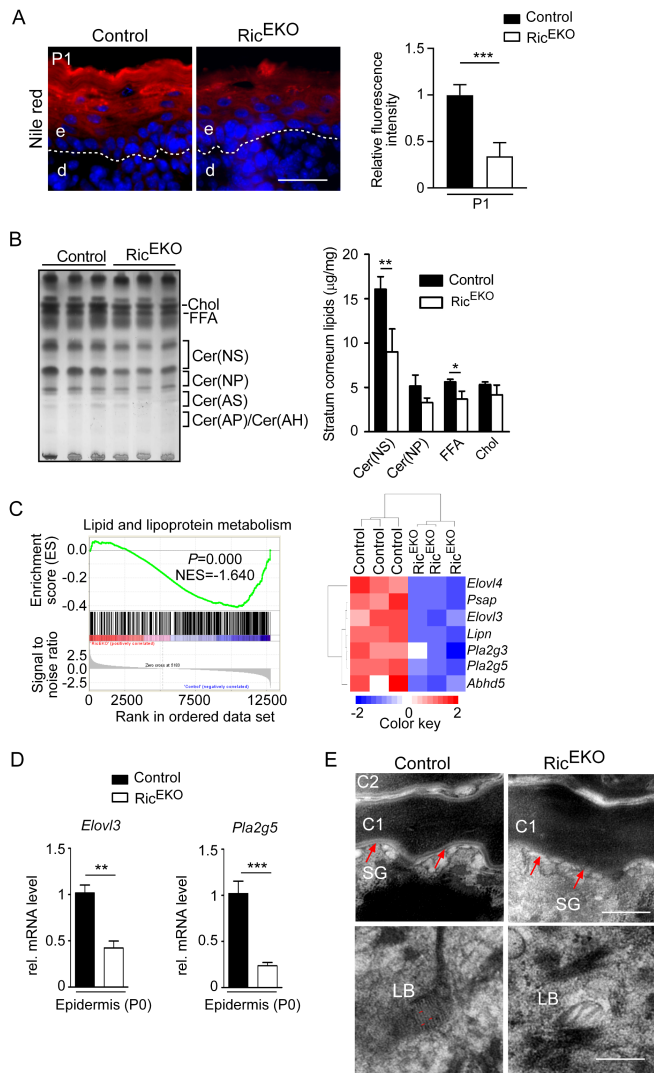


Figure 4

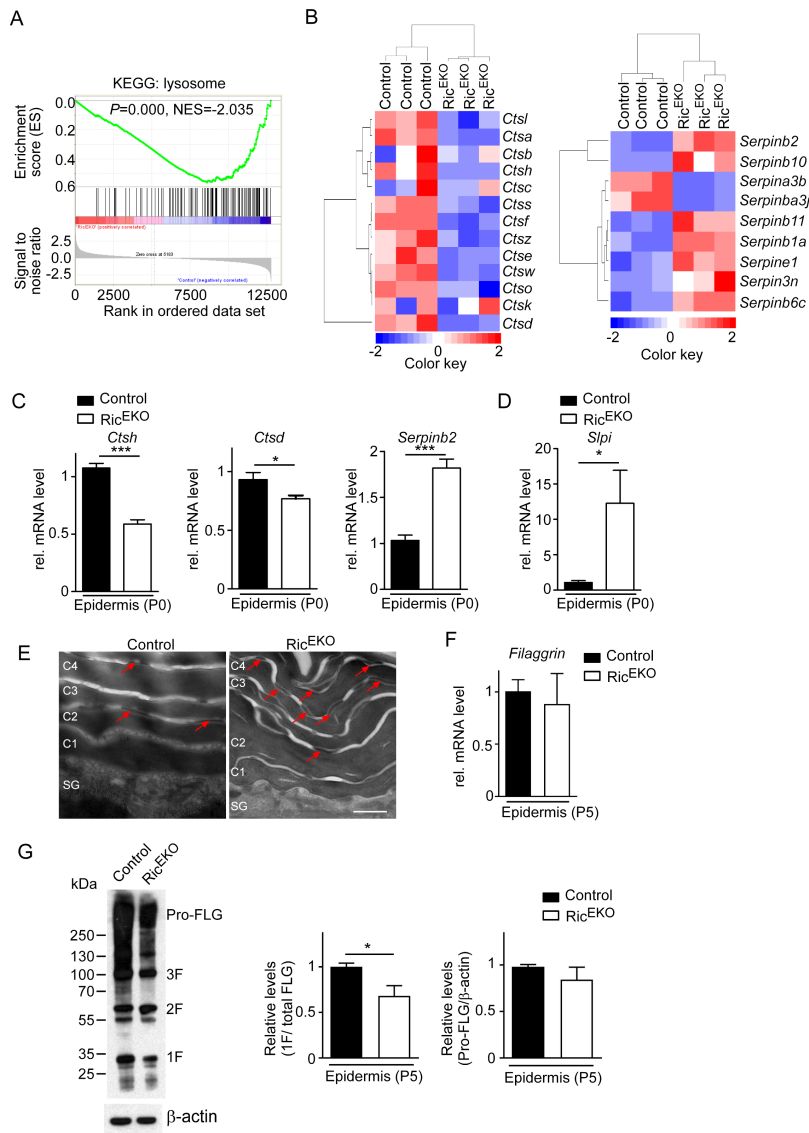


Figure 5

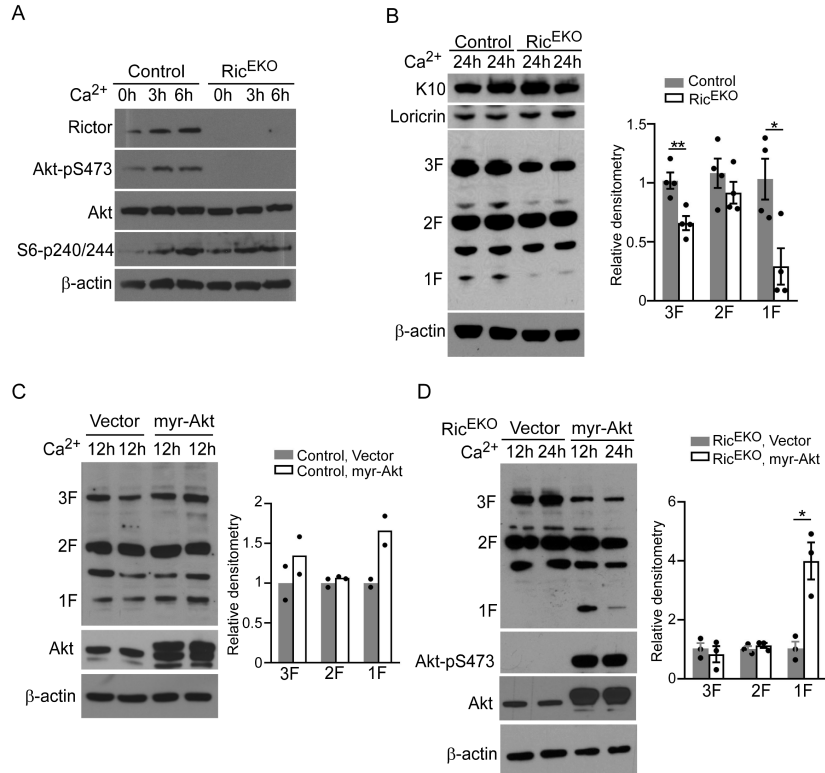




Figure 6

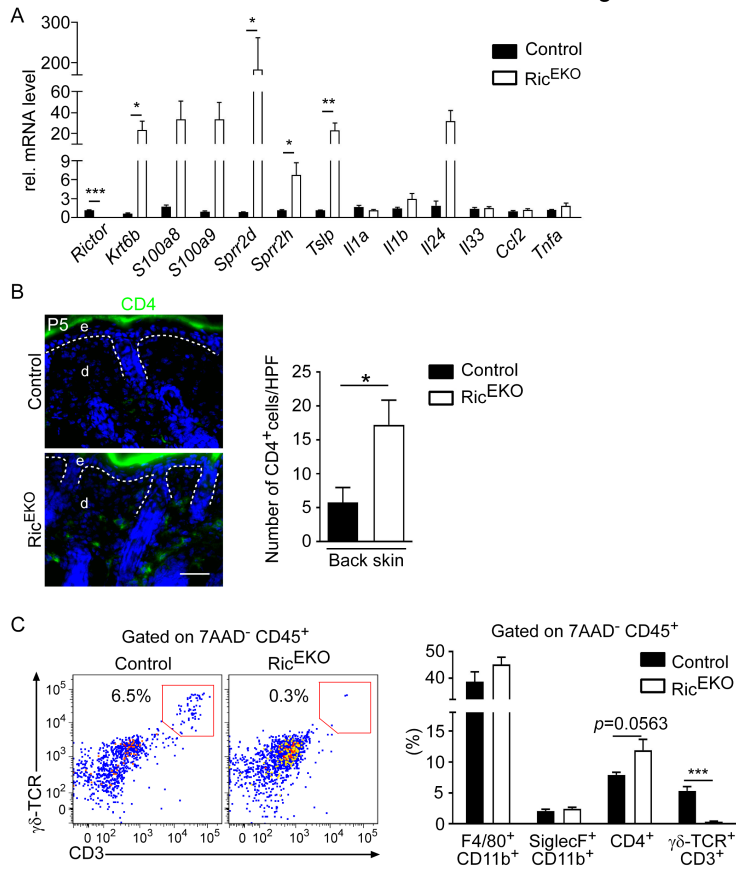


Figure 7

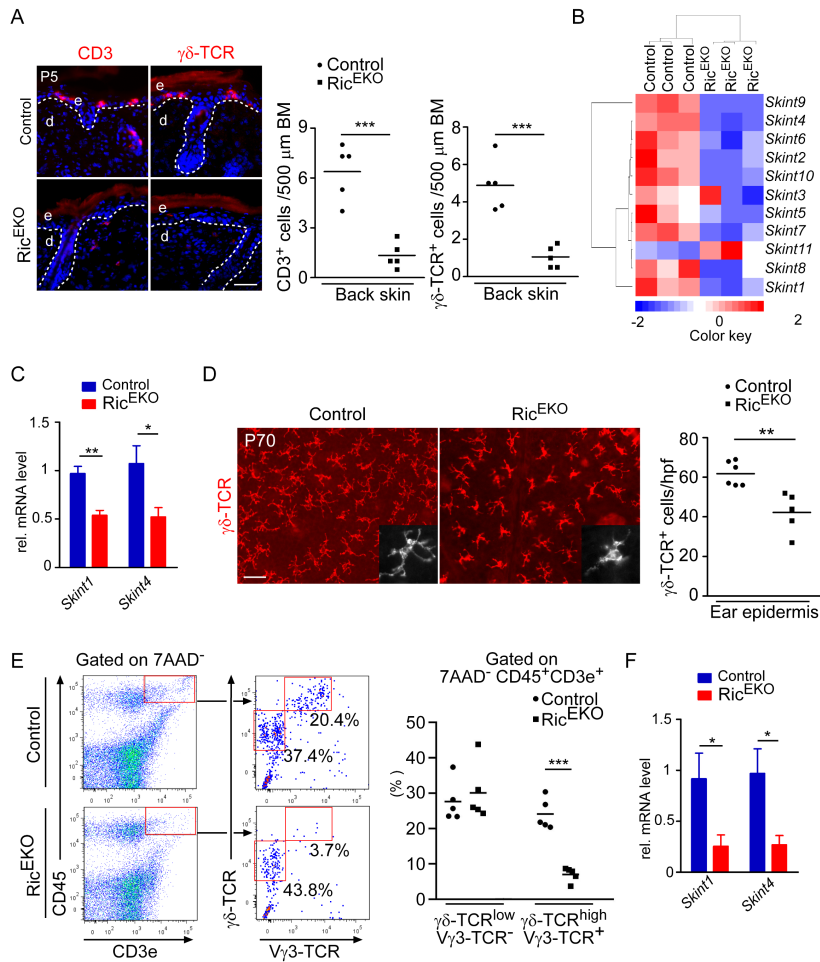
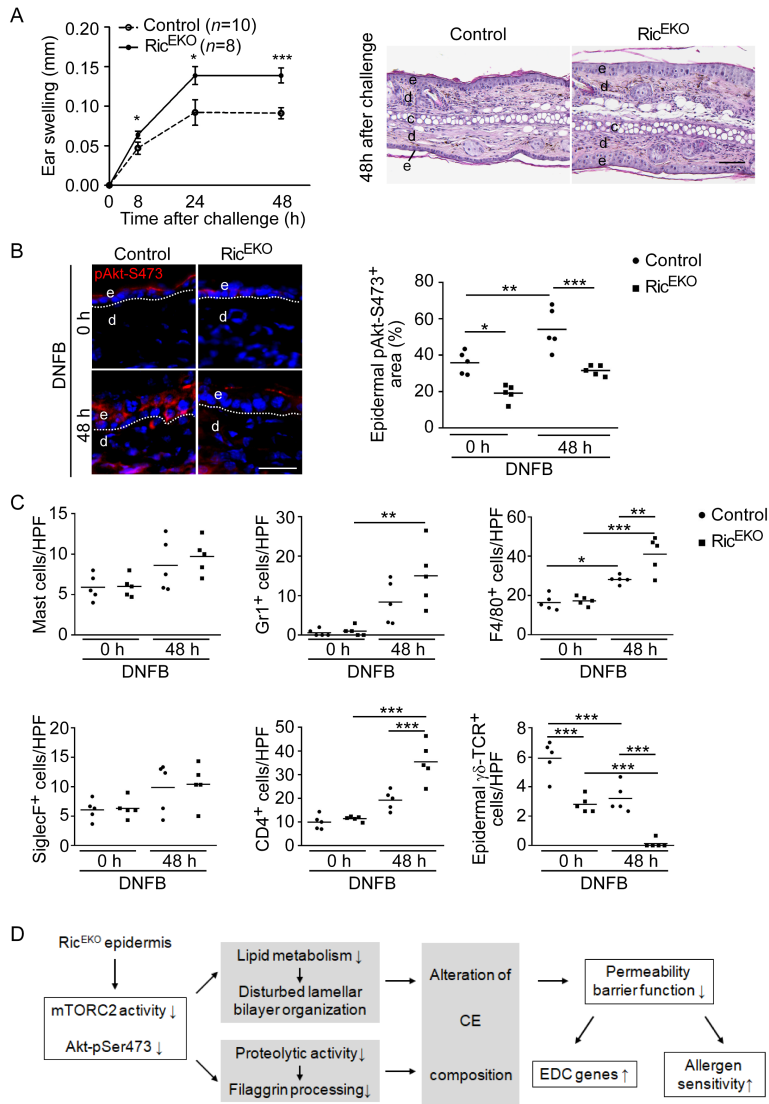


Figure 8



## Online Repository

### **Epidermal mTORC2 controls lipid synthesis and filaggrin processing in epidermal barrier formation**

Xiaolei Ding, PhD<sup>1,2</sup>, Sebastian Willenborg, PhD<sup>1</sup>, Wilhelm Bloch, PhD<sup>3</sup>, Sara A. Wickström, MD, PhD<sup>4,5,6,7</sup>, Prerana Wagle, MSc<sup>7</sup>, Susanne Brodesser, PhD<sup>7</sup>, Axel Roers, MD<sup>8</sup>, Alexander Jais, PhD<sup>9</sup>, Jens C. Brünig, MD<sup>2,7,9</sup>, Michael N. Hall, PhD<sup>10</sup>, Markus A. Rüegg, PhD<sup>10</sup>, Sabine A. Eming, MD<sup>1,2,7</sup>

<sup>1</sup>Department of Dermatology, University of Cologne, Kerpenerstr. 62, 50937 Cologne, Germany

<sup>2</sup>Center for Molecular Medicine Cologne (CMMC), University of Cologne, 50931 Cologne, Germany

<sup>3</sup>Department of Molecular and Cellular Sport Medicine, German Sport University Cologne, 50933 Cologne, Germany

<sup>4</sup>Paul Gerson Unna Group 'Skin Homeostasis and Ageing', Max Planck Institute for Biology of Ageing, 50931 Cologne, Germany

<sup>5</sup>Helsinki Institute of Life Science, Biomedicum Helsinki, University of Helsinki, FI-00014 Helsinki, Finland

<sup>6</sup>Wihuri Research Institute, Biomedicum Helsinki, University of Helsinki, FI-00014 Helsinki, Finland

<sup>7</sup>Cluster of Excellence Cellular Stress Responses in Aging-associated Diseases (CECAD), University of Cologne, 50931 Cologne, Germany

<sup>8</sup>Institute for Immunology, Medical Faculty Carl Gustav Carus, TU Dresden, 01307

Dresden, Germany

<sup>9</sup>Max Planck Institute for Metabolism Research, Gleueler Strasse 50, 50931 Cologne,

Germany

<sup>10</sup>Biozentrum, University of Basel, CH-4056 Basel, Switzerland

Corresponding author:

Sabine A. Eming, MD

Professor of Dermatology

Department of Dermatology

University of Cologne

Kerpenerstr. 62

50937 Cologne

Germany

Phone: ++49-221-4783196

Fax: ++49-221-4785949

E-mail: [sabine.eming@uni-koeln.de](mailto:sabine.eming@uni-koeln.de)

### **Supplemental Materials**

Supplemental Figure 1. Conditional targeting *Rictor* gene in epidermal keratinocytes.

Supplemental Figure 2. Immune cell composition and gating strategies for FACS analysis of cell suspensions isolated from back skin and ear.

Supplemental Figure 3. Mild skin inflammation in naïve Ric<sup>EKO</sup> mice under SPF conditions.

Supplemental Figure 4. Immune cell infiltration in ear skin tissue.

Supplemental Figure 5. Gene expression analysis in ear skin tissue.

Supplemental Table 1: Antibodies used for immunostaining and Western blot analysis

Supplemental Table 2: Primer sequence used for qRT-PCR analysis

Supplemental Table 3: Genes in biological processes (BP) identified by GO term analysis.

## Supplemental Figure legends

### Supplemental Figure 1. Conditional targeting *Rictor* gene in epidermal keratinocytes.

(A) Scheme illustrating the *Rictor* gene construct, the 2 loxP sites flanking exons, and the PCR fragment length before and after recombination. (B) PCR product of genomic DNA isolated from various tissues. (C) Phospho-Akt (Akt-pS473) immunostaining of back skin of control and Ric<sup>EKO</sup> at P5; scale bar, 25  $\mu$ m. (D) Survival curve of control ( $n=16$ ) and Ric<sup>EKO</sup> ( $n=15$ ) mice. Mantel-Cox test was used to calculate the P value. (E) Representative H&E-stained back skin sections from control and Ric<sup>EKO</sup> mice at P70. Scale bar, 25  $\mu$ m. (F) TEWL in Ric<sup>EKO</sup> and control mice. (G) Representative immunofluorescence staining at P5 for ZO-1, E-cadherin (E-cad), Desmoplakin1/2 (DSP1/2), Desmoglein1/2 (DSG1/2),  $\beta$ 4-integrin (red); white dashed lines indicates basement membrane; nuclei are visualized with DAPI (blue); scale bar, 20  $\mu$ m. (H) Body weight of control ( $n=8$ ) and Ric<sup>EKO</sup> ( $n=7$ ) mice at different ages. (I) Ultrastructural analysis of back skin epidermis of control and Ric<sup>EKO</sup> mice at P5. Lower panel: higher magnification images show desmosome (de) structure. e, epidermis; d, dermis; SC, stratum corneum; SG, stratum granulosum; SS, stratum spinosum; SB, stratum basale, scale bar, 5  $\mu$ m (upper panel) and 100 nm (lower panel). Each dot or square represents one mouse. Data are presented as mean or as mean  $\pm$  s.e.m; unpaired t-test was used to calculate the P value; \*\* $P < 0.01$ ; \*\*\* $P < 0.001$ .

**Supplemental Figure 2. Immune cell composition and gating strategies for FACS analysis of cell suspensions isolated from back skin and ear.**

(A) Left: Representative Giemsa staining and F4/80 immunostaining with back skin sections from control and Ric<sup>EKO</sup> mice at P5. Right: quantification of mast cells and F4/80<sup>+</sup> macrophages cells per high-power field (HPF) ( $n=5$  per genotype). Scale bar, 25  $\mu\text{m}$ ; data are presented as mean  $\pm$  s.e.m. (B) Representative FACS analysis of single cell suspensions of back skin in control and Ric<sup>EKO</sup> mice (P5). Upper panel: single cells were gated (G1-3) and analyzed for 7-AAD staining and expression of CD45 (G4). Lower panel: 7-AAD<sup>-</sup>CD45<sup>+</sup> cells (G4) were analyzed for expression of (from left to right) CD3 and  $\gamma\delta$ -TCR, CD4, CD11b and F4/80, and CD11b and Siglec F. (C) Representative FACS analysis of single cell suspensions of ear skin in control and Ric<sup>EKO</sup> mice (P70). Single cells (G1-3) and 7-AAD<sup>-</sup> cells (G4) were gated. Red polygons indicate the gate and percentages indicate the proportion of gated cells. FSC-A, forward scatter area; FSC-H, forward scatter height; G, gate; SSC-A, sideward scatter area; SSC-H, sideward scatter height.

**Supplemental Figure 3. Mild skin inflammation in naïve Ric<sup>EKO</sup> mice under SPF conditions.**

(A) Representative macroscopic appearance of control and Ric<sup>EKO</sup> mice at P70. (B) Quantification of CD4<sup>+</sup>, mast cells (MCs), and F4/80<sup>+</sup> macrophages in back skin sections from control and Ric<sup>EKO</sup> mice at P70 ( $n=5$  per genotype). (C) qRT-PCR analysis of *Il6*, *Tnfa*, *Il1b*, and *Tslp* expression in Ric<sup>EKO</sup> and control skin at P70 ( $n=5$  per genotype). (D) Serum IgE amount in Ric<sup>EKO</sup> and control mice were determined by ELISA ( $n=6$  per



genotype) at P70. (E) Croton oil-induced irritated contact dermatitis (ICD) response. Ear swelling of control and Ric<sup>EKO</sup> animals after topical application of croton oil was calculated and shown ( $n=5$  per genotype). Data are presented as mean  $\pm$  s.e.m.

**Supplemental Figure 4. Immune cell infiltration in ear skin tissue.** Representative Giemsa stainings and immunohistochemical stainings for Gr1, F4/80, Siglec F, CD4 and  $\gamma\delta$ -TCR of untreated (DNFB, 0 h) and treated (DNFB, 48 h) ear sections from control and Ric<sup>EKO</sup> mice ( $n=5$ ). Arrows indicate mast cells (Giemsa stain, purple) or polymorphonuclear cells (Gr1 stain, brown) and dashed line indicates the border between epidermis and dermis. e, epidermis; d, dermis; scale bar, 25  $\mu$ m.

**Supplemental Figure 5. Gene expression analysis in ear skin tissue.**

qRT-PCR analysis of stress response gene (*Krt6b*, *S100a8* and *Sprr2d*) and inflammatory mediator (*Il6*, *Tnfa* and *Il24*) expression in untreated (DNFB, 0 h) and treated (DNFB, 24 h) ear skin tissues from control and Ric<sup>EKO</sup> mice ( $n=6$  per genotype). Gene expression in untreated control ear skin was referred as 1 and relative fold changes were analyzed and shown. Data are presented as mean  $\pm$  s.e.m; ANOVA one-way test analysis with Bonferroni multiple comparison test was used; \* $P < 0.05$ ; \*\* $P < 0.01$ ; \*\*\* $P < 0.001$ .

**Supplemental Table 1: Antibodies used for immunostaining and Western blot analysis**

<i>Name</i>	<i>Catalog number</i>	<i>Source</i>
<i>Primary antibodies used for immunostaining</i>		
Akt-pS473	9271	Cell Signaling, Beverly, MA
CD4	14-0042-85	Thermo Fisher Scientific
Ly-6G and Ly-6C (Gr1)	550291	BD Biosciences
Siglec F	552126	BD Biosciences
CD3	MCA1477	AbD Serotec
F4/80	MOF4F (V500)	Dianova
ZO-1	(hybridoma) Rat, Clone R26.4C	Stevenson BR et al., 1986
Desmoglein1/2	61002	Progen
Desmoplakin1/2	61003	Progen
$\beta$ 4-integrin	555719	BD Biosciences
E-cadherin	610182	BD Biosciences
$\gamma\delta$ T-Cell Receptor	553175	BD Biosciences
<i>Secondary antibodies used for immunostaining</i>		
Anti-rabbit IgG Alexa Fluor® 488	A-32731	Thermo Fisher Scientific
Anti-rabbit IgG Alexa Fluor® 568	A-11011	Thermo Fisher Scientific
Anti-rat IgG Alexa Fluor® 488	A-11006	Thermo Fisher Scientific
Anti-mouse Alexa Fluor® 594	A-11032	Thermo Fisher Scientific
Anti-rabbit IgG HRP	K4003	DAKO

<i>Primary antibodies used for Western blot</i>		
S6-pS240/244	5364	Cell Signaling, Beverly, MA
Rictor	2140	Cell Signaling, Beverly, MA
Akt-pS473	9271	Cell Signaling, Beverly, MA
Loricrin	PRB-145P	Covance, Princeton, New York
Filaggrin	PRB-417P	Covance, Princeton, New York
Akt	9272	Cell Signaling, Beverly, MA
Keratin 10	PRB-159P	Covance, Princeton, New York
$\beta$ -actin (C4)	MAB1501	Sigma-Aldrich
$\alpha$ -Tubulin (B-5-1-2)	T6074	Sigma-Aldrich
<i>Secondary antibodies used for Western blot</i>		
Anti-rabbit-IgG-HRP	P0448	DAKO
Anti-mouse-IgG-HRP	P0161	DAKO

**Supplemental Table 2: Primer sequence used for qRT-PCR analysis**

<i>Gene</i>	<i>Forward primer</i>	<i>Reverse primer</i>
<i>GAPDH</i>	CATGTTTGTGATGGGTGTGA	AATGCCAAAGTTGTCATGGA
<i>Nrf2</i>	CCATTCCCGAATTACAGTGTCTTA	CGCCAAAATCTGTGTTTAAGGTG
<i>Sfn</i>	CCGAACGGTATGAAGACATGG	CGGTACTTTCACCTCGGG
<i>Slc7a11</i>	CAACAAAGATCGGGACTGCT	GCTGGCTGGTTTTACCTCAA
<i>Srxn1</i>	CGGTGCACAACGTACCAAT	TTGATCCAGAGGACGTCGAT
<i>Sprr2d</i>	CTGGTACTCAAGGCCGAGAC	CAGGGCACTTTGGTGGAG
<i>Sprr2e</i>	CAGGTCCTAGGCTACTTTGGAG	ACTGTGGATGAGGACAAGGC
<i>Sprr2h</i>	GACACTTGGTACTCAAGCTCTGG	TGCACTGCTGCTGTTGGTAA
<i>Rptm</i>	TCCTGCCTCTTCTGCTCATT	AGCGCCTACCCCATGATATT
<i>Lce3f</i>	TCCTGGCTCTCCTGTTCTC	CCCAGGCAGTTATCAAAAGC
<i>S100a8</i>	GCCGTCTGAACTGGAGAAG	GTGAGATGCCACACCCACTT
<i>Keratin6b</i>	TGCAGACGAGATCAACTTCC	TGCAGACGAGATCAACTTCC
<i>Elov13</i>	CTGTTGCTCATCGTTGTTGG	GCTTGAGGCCCACTGTAAAC
<i>Pla2g5</i>	CTCACACTGGCTTGGTTCCT	CATAACAACGGTTCGTGCATC
<i>Ctsh</i>	CACGGAGACGGAGTTACCAG	GTGGCCATTACTCCTGCT

<i>Ctsd</i>	AATCCCTCTGCGCAAGTTCA	CACTGGCTCCGTGGTCTTAG
<i>Sipi</i>	CGGCAAATACAAGTGCTGTG	CCTGGGAGCAGGGAAGTAGT
<i>Serpinb2</i>	TGCCAGCTTTCCAAGAAGCATT	AGATTGAGGGCAAACATGGTG
<i>Rictor</i>	GAGAAAGCTGGGCCATCTGA	AACCCGGCTGCTCTTACTTC
<i>Tslp</i>	TCTCAGGAGCCTCTTCATCCT	CTCACAGTCCTCGATTTGCTC
<i>Il-1<math>\alpha</math></i>	GTCGGGAGGAGACGACTCTA	TGGTCACAAACAGTGGGAGG
<i>Il-1<math>\beta</math></i>	GGACCCCAAAGATGAAGGGCTGC	GCTCTTGTGATGTGCTGCTGCG
<i>Il-24</i>	TGCCAAGTGACAGGGGTGGTTCT	CAGCACCCGAGACATTCCGCAG
<i>Il-33</i>	TGATCAAAGAGGCCGGGAAC	ACGCAGATTCCGCCTTTACA
<i>Ccl2</i>	TCCACGTGTTGGCTCAGCCAG	CCAGCCTACTCATTGGGATCATCTT
<i>Tnf-<math>\alpha</math></i>	GACCCTCACACTCAGATCATCTTCT	CCTCCACTTGGTGGTTTGTCT

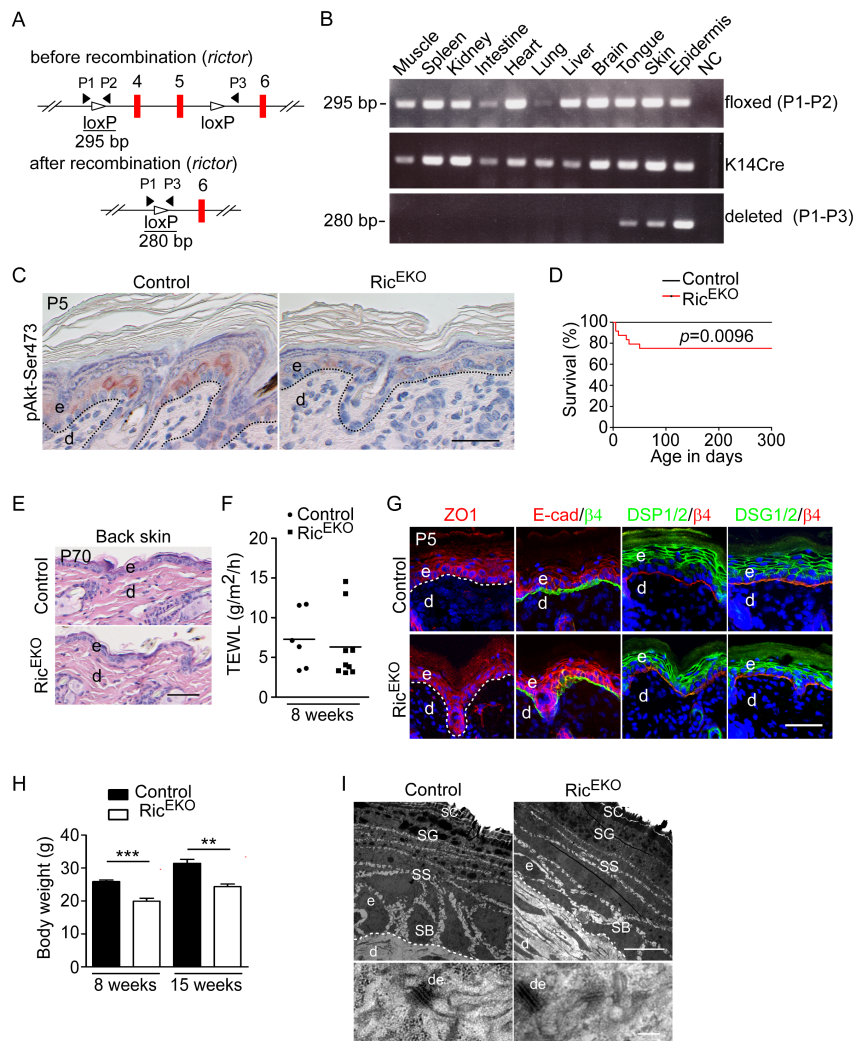
**Supplemental Table 3. Related to Figure 3. Differentially expressed genes in GO term analysis identified biological processes (BP). Gene ontology Enrichment analysis (GO) of differentially regulated transcripts from Ric<sup>EKO</sup> vs. control comparison using DAVID 6.8 online software. Only genes that have fold change >1.5 and a *P* value < 0.05 were used.**

BP	Up-regulated genes in Ric <sup>EKO</sup> epidermis
Peptide cross-linking	LCE3A, LCE3B, LCE3C, COL3A1, LCE3D, SPRR2H, SPRR2F, SPRR2E, SPRR2K, SPRR2I, LCE1J, SPRR2D, SPRR1A, SPRR2A3, SPRR1B, SPRR2B, TGM1, SPRR2A2, SPRR3, LCE3F, LCE3E, THBS1, LCE1K
Keratinization	KRT6A, KRT6B, SPRR2H, SPRR2F, SFN, SPRR2E, SPRR2K, SPRR2I, KRT17, KRT16, SPRR2D, SPRR1A, SPRR2A3, SPRR1B, CNFN, SPRR2B, TGM1, SPRR2A2, SPRR3
Keratinocyte differentiation	PTGS2, LCE3A, LCE3B, LCE3C, LCE3D, SPRR2H, SPRR2F, SFN, SPRR2E, SPRR2K, SPRR2I, LCE1J, KRT16, SPRR2D, SPRR1A, SPRR2A3, SPRR1B, SPRR2B, TGM1, SPRR2A2, SPRR3, LCE3F, LCE3E, LCE1K
Wound healing	DCBLD2, KRT6A, NOG, S100A8, TNC, COL3A1, CXCL2, TGFB2, IL24, ELK3, AQP1, TPM1, MMP12, TIMP1, MACF1, CCL20, SERPINE1, SERPIN2, TGFA, CNN2, LOX, COL1A1, NBEAL2
Cell adhesion	CADM4, VCL, NOV, CGREF1, COL12A1, CYR61, KIRREL3, BYSL, CDHR1, ADGRE5, FBLIM1, THY1, TNFAIP6, BVES, HAS1, VCAN, LAMC2, MFAP4, TNFRSF12A, TNC, ITGB4, ITGB1, DCHS1, PTK2B, ITGB6, COL6A2, COL6A1, THBS1, THBS2, THBS3, DPT, COL18A1, PODXL, ITGA3, TINAGL1, PCDH17, COL5A1, LYVE1, COL19A1, CASS4, ITGA6, ITGA5, DSG3, PKP4, ITGA7, SULF1, DSC2, ABL2, NTM, MYH10

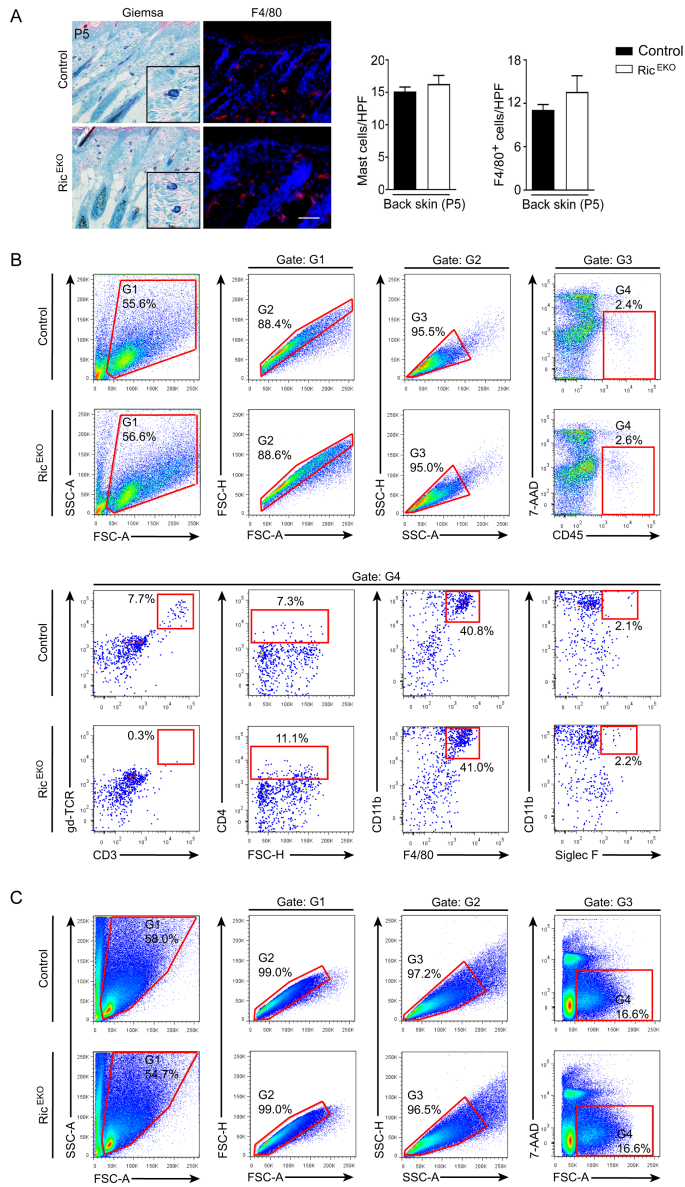
BP	Down-regulated genes in Ric <sup>EKO</sup> epidermis
Immune system process	LY86, TLR1, LY9, C1QC, SKAP1, ISG20, TLR9, OASL2, OASL1, CLEC4A2, CD300C2, CD3E, PRG2, PIK3CD, PADI4, TRAT1, CD84, C1QA, C1QB, H2-AA, CD300LF, TXK, RNF135, TNFAIP8L2, KLRK1, UNC93B1, SP110, OAS2, IL34, RNF125, NAIP5,

	PSTPIP1, ZAP70, MR1, CSF1R, CD7, ZBP1, ITK, CARD9, THEMIS, HCK, TNFRSF13C, CTLA4, TRIL, FCGR1, PSMB9, IFIT3, LAT, IFIT2, H2-EB1, C1RL, THEMIS2
Lipid metabolic process	ACOX2, PPARA, ALOX12E, HINT2, BSCL2, 4833423E24RIK, GPCPD1, ACOX3, FAR2, INSIG2, APOE, ELOVL3, NPC1L1, CES1D, FA2H, PLD4, DECR1, LPCAT2, PNPLA5, HSD11B1, NEU3, THEM5, AKR1D1, PLA2G5, HACL1, ECH1, HSD17B2, ABHD3, CERS4, ACSBG1, PLIN5, ACSL4, ACAA1B, GAL3ST1, ACSL6, SCD1, SOAT1, PLA2G16, SCD3, A4GALT, PLB1, CYP46A1, ACER2, ACER1, FADS3, SPTSSB, FAM213B, ACACB, CRAT, FADS6, GDPD1, AWAT2, ACSM3, AWAT1, ACSM2, ACSM1, LIPC
Metabolic process	ACOX2, ARSB, ALAD, ARSG, HEXB, ECHDC1, GM436, ACOX3, UGT1A7C, UGT1A6B, PHOSPHO1, 9430007A20RIK, ACOXL, NEIL2, FBP1, ALDH3B2, LPCAT2, UGT1A1, PNPLA5, AADAC, CAMK1, NEU3, ALPL, ECH1, GM5538, ISOC2B, HSD3B6, UGT3A1, UGT3A2, ACSBG1, C130079G13RIK, ALDH1A1, ALDH1A7, ACSL4, ACAA1B, FAHD2A, ACSL6, GSTA2, GSTA3, ACY3, PM20D1, NPL, GM13124, ACACB, ENGASE, CPS1, ACSM3, ACSM2, ACSM1, LYG2, ARSA, GM13178, GM13177, ACAD10
Fatty acid metabolic process	ACOX2, PPARA, ECH1, ALOX12E, 4833423E24RIK, ACSBG1, ACOX3, CRYL1, ELOVL3, ACSL4, ACAA1B, ACSL6, SCD1, SCD3, ACOXL, FA2H, FADS3, FAM213B, ACACB, DECR1, CRAT, FADS6, ACSM3, ACSM2, ACSM1, LIPC, THEM5
Innate immune response	TNFAIP8L2, LY86, TLR1, KLRK1, UNC93B1, SP110, TRIM15, OAS2, LY9, IL34, C1QC, TLR9, ISG20, OASL2, NAIP5, OASL1, ZAP70, PSTPIP1, FCER1G, CLEC4A2, MR1, CSF1R, TYROBP, ZBP1, ITK, CARD9, HCK, PIK3CD, PADI4, TRIL, FCGR1, IFIT3, CD84, C1QA, IFIT2, C1QB, CYBB, C1RL, TXK, TREM2, RNF135

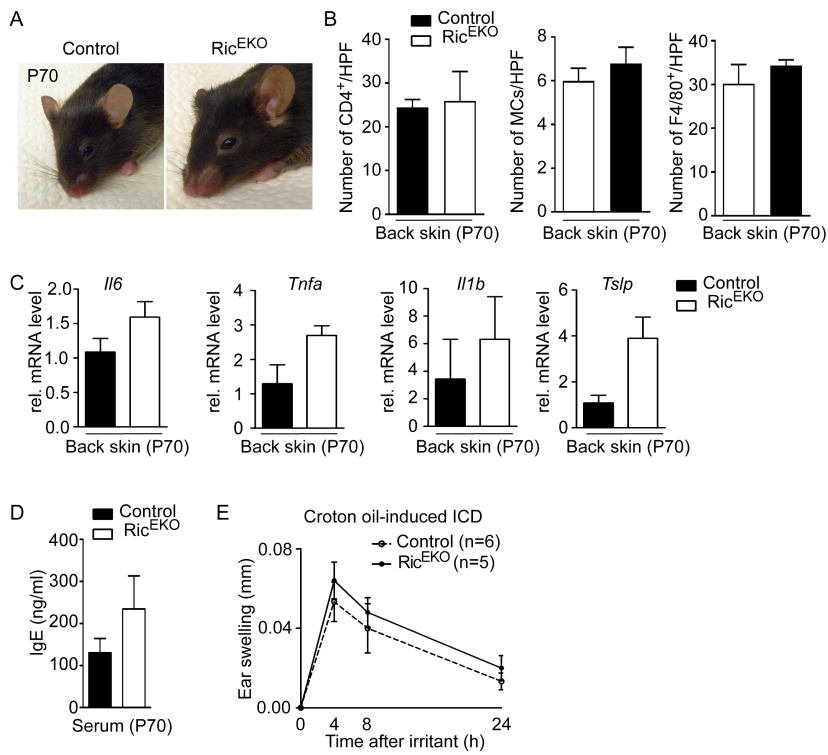
## Supplemental Figure 1



Supplemental Figure 2

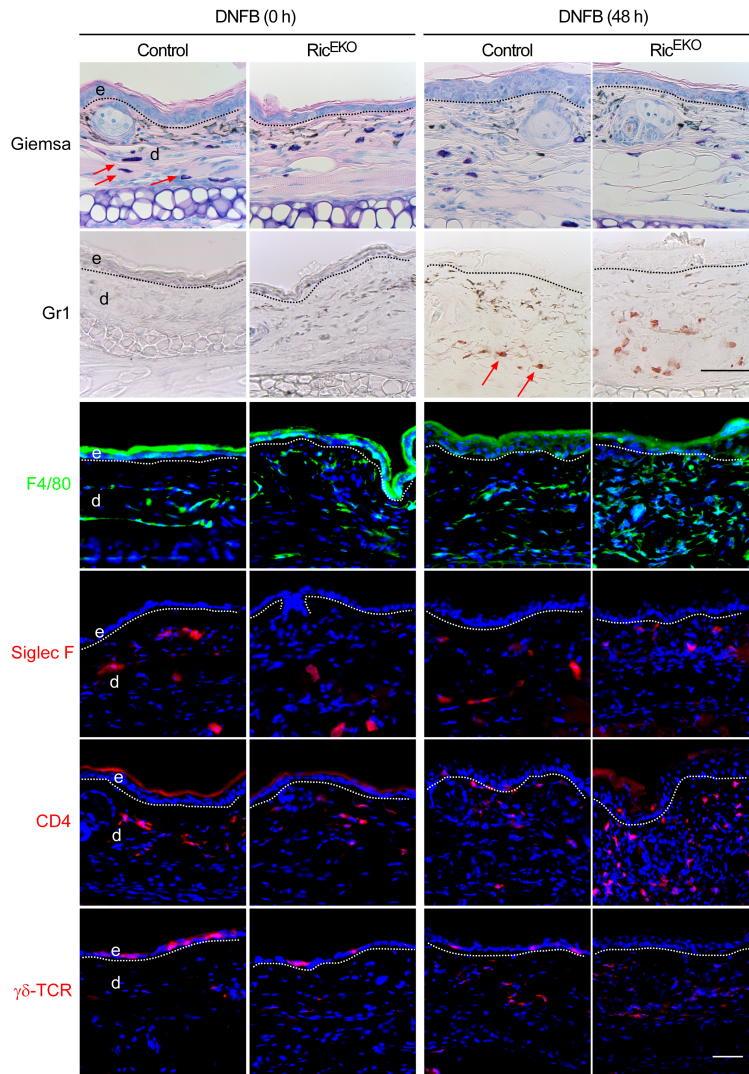


Supplemental Figure 3





Supplemental Figure 4



Supplemental Figure 5

